Nutrient transport in bioreactors for bone tissue growth : why do hollow fiber membrane bioreactors work

Nutrient Transport in Bioreactors for Bone Tissue Growth: Why Do Hollow Fiber Membrane Bioreactors Work

N.S. Abdullah[1,2], D.R. Jones[1] and D.B. Das[3,*]

[1]Department of Engineering Science, University of Oxford, Oxford OX1 3PJ, UK

[2]School of Materials and Mineral Resources Engineering, Engineering Campus, Universiti Sains Malaysia, 14300 Nibong Tebal, Penang, Malaysia

[3]Department of Chemical Engineering, Loughborough University, Loughborough LE11 3TU, UK

Revised Paper Submitted for Consideration of Publication in the Journal:

Chemical Engineering Science

18 August, 2008

[*]**Author for correspondence** **(Email: D.B.Das@lboro.ac.uk)**

Nutrient Transport in Bioreactors for Bone Tissue Growth: Why Do Hollow Fiber Membrane Bioreactors Work

N.S. Abdullah[1,2], D.R. Jones[1] and D.B. Das[3]

[1]Department of Engineering Science, University of Oxford, Oxford OX1 3PJ, UK
[2]School of Materials and Mineral Resources Engineering, Engineering Campus, Universiti Sains Malaysia, 14300 Nibong Tebal, Penang, Malaysia
[3]Department of Chemical Engineering, Loughborough University, Loughborough LE11 3TU, UK

Abstract

One of the main aims of bone tissue engineering is to produce three-dimensional soft bone tissue constructs of acceptable clinical size and shape in bioreactors. The tissue constructs have been proposed as possible replacements for diseased or dysfunctional bones in the human body through surgical transplantations. However, because of certain restrictions to the design and operation of the bioreactors, the size of the tissue constructs attained are currently below clinical standards. We believe that understanding the fluid flow and nutrient transport behaviour in the bioreactors is critical in achieving clinically viable constructs. Nevertheless, characterization of transport behaviour in these bioreactors is not trivial. As they are very small in size and operate under stringent conditions, in-situ measurements of nutrients are almost impossible. This issue has been somewhat resolved using computational modelling in previous studies. However, there is still a lack of certainty on the suitability of bioreactors. To address this issue we systematically compare the suitability of three bioreactors for growing bone tissues using mathematical modelling tools. We show how nutrient transport may be improved in these bioreactors by varying the operating conditions and suggest which bioreactor may be best suited for operating at high cell densities in order to achieve soft bone tissues of clinical size. The governing equations defined in our mathematical frameworks are solved through finite element method. The results show that the hollow fiber membrane bioreactor (HFMB) is able to maintain higher nutrient concentration during operation at high cell densities compared to the other two bioreactors, namely suspended tube and confined profusion type bioreactor. Our results show that by varying the operating conditions nutrient transport may be enhanced and the nutrient gradient can be substantially reduced. These are consistent with previous claims suggesting that the HFMB is suited for bone tissue growth at high cell densities.

Keywords

Nutrient transport, bioreactors, Krogh cylinder approximation, Navier-Stokes equations, convection-diffusion-reaction equations, finite element modelling.

1. Introduction

The worldwide need for bone replacements is currently critical. This is because the natural substitutes for dysfunctional or damaged bones are limited compared to the number of medical cases that seek bone replacements. Furthermore, the current alternatives of autografting, allografting or inserting man-made materials are associated with many problems and may need medical attention after some time (Abdullah and Das, 2007; Ye et al., 2006; Vance et al. 2005; Fleming et al., 2000; Lanza et al., 1997; Yaszemski et al., 1996). Bone tissue engineering (BTE) promises a new route towards repair, restoration and regeneration of dysfunctional or impaired bones (Hollinger et al., 2005; Fleming et al., 2000; Lanza et al., 1997). BTE protocols allow bone tissues to be grown in bioreactors, which promise to provide natural and inexhaustible supply of replacements for damaged bones. Excellent reviews on BTE can be found in the literature (e.g., Abdullah et al., 2006; Chong and Chang, 2006; Nerem, 2006; Ye et al., 2006, 2004; Cortesini, 2005; Meyer et al., 2004a,b; Cancedda et al., 2003; Rose and Oreffo, 2002; Lanza et al., 1997). It is clear from these literatures that efforts have been proven successful for artificial bone tissue growth in laboratories. However, attaining constructs of clinical size is still a problem. Current bone tissue constructs are less than 0.5mm thick, which is still far from general clinical need of 2-5mm (Ye et al., 2006; Martin and Vermette, 2005; Freed and Vunjak-Novakovic, 1998).

Please note that bone tissues, being mammalian tissues, rank among the most difficult tissues to grow under in vitro reactor conditions. This is because these tissues have critical nutrient needs, are sensitive to wastes of metabolic reactions and are highly fragile to shear stresses (Freshney, 2000; Smalt et al., 1997; Hillsley and Frangos, 1994). Hence, the bioreactors for BTE applications are expected to provide (i) physical support and protection to the tissues from forces acting on them and (ii) excellent mass transport for nutrients and wastes. This is especially so in case for growing bone tissues as bone cells may be found situated deep in the mineralized bone matrix. In the human body, ample nutrient distribution is achieved by having a complex network of blood vessels that penetrates through the mineralized bone matrix. Without these blood vessels, sufficient nutrient supply poses a huge challenge (Ye et al., 2006, 2004; Martin and Vermette, 2005).

In addressing these challenges in artificial conditions, bioreactor designs have evolved significantly so that high nutrient concentrations can be maintained during their operation. Thus, many types of bioreactors have been introduced for growing bone tissues (Martin and Vermette, 2005; Wiesmann et al., 2004). It emerges from the review of these work that there are three main types of bioreactors which could be used for BTE applications. The first,

simplest and most widely used bioreactor are based on culture dishes and flasks (Martin and Vermette, 2005; Wiedmann-Al-Ahmad et al., 2002). They are easy to handle and fabricate and, cheaper compared to other types of bioreactors. A sample reactor that falls in this category is the suspended tube bioreactor (STB). As depicted in Figure 1, the STB is a batch process with cells seeded on a scaffold construct in the reactor flask which is submerged in a nutrient rich medium. In general, these bioreactors have high nutrient limitations and are unable to produce 3-D bone constructs. Furthermore, for large sized cell-filled porous scaffolds, high concentration of nutrient in the surrounding media coupled with poor transport mechanisms will create a severe nutrient gradient. As a result, cells inside the porous scaffold migrate (e.g., chemotaxis) to regions where nutrient concentration are higher. This creates a problem of inhomogeneous spatial distribution of cells in the extracapillary space (ECS) (Sengers et al., 2007). Sizeable 3-D bone tissue constructs of clinical value cannot be achieved this way. Although apparently that is the claim, no specific studies were made to compare the performance of the culture dishes and flasks (e.g., STB) at high cell densities to other bioreactors for BTE. Being the most primitive, simple and most widely used type of bioreactor, comparison between these and other type of bioreactors warrants some interest. This may include questions such as how mass transport can be improved in different bioreactors from a system which relies truly by diffusion alone, and with addition of perfusion.

Since batch systems are not very effective for growing 3D bone tissues with high cell densities, a number of perfused bioreactors have been designed. These bioreactors operate with less need of manual handling as nutrient media can be pumped in and out of the systems. An example of a perfused bioreactor is the confined perfusion bioreactor (CPB), as shown in Figure 2. Further technical improvements in the area of in vitro bone tissue engineering have led to the development of more sophisticated bioreactor systems. Bioreactors for bone tissue growth promise now to mimic the physical conditions in the human body (Abdullah et al., 2006; Ye et al., 2006) and bone morphology (Wiesmann et al., 2004, 1997). One example of such a bioreactor is the hollow fiber membrane bioreactor (HFMB). The HFMB consists of a hollow fiber (HF) bundle contained in an external housing. The cells are cultured in the ECS. A porous scaffold is placed in the ECS where cells attach to and proliferate. Nutrients are supplied by flowing media through the fiber lumen, which allow nutrient diffusion to the ECS across the fiber membranes. It has been claimed that the HFMB design offers better mass transfer behaviour as the HFs enable nutrients to be supplied to the centre of the bone tissues, mimicking the in-vivo blood vessels in human bones (Abdullah and Das, 2007; Das, 2007; Ye et al., 2006, 2004; Martin and Vermette, 2005). This promises to minimize mass transfer

limitations and enhance the possibility of growing thick bone tissue (3D). Figure 3 shows a single HF, depicted as a Krogh cylinder in the HFMB.

Other perfused culture systems have also been documented, including spinner flasks (Gooch et al., 2001; Carrier et al., 1999; Vunjak-Novakovic et al., 1998) and rotary vessels (Chen and Hu, 2006; Detamore and Athanasiou, 2005; Qiu et al., 1999). The limitation with both of these systems is that mixing at the surface of the scaffolds may not be sufficient to deliver the necessary nutrients to the interior of the scaffold. Although attempts are made for bone tissue growth and regeneration (Chen and Hu, 2006; Detamore and Athanasiou 2005), the spinner flasks are usually operated at low cell numbers due to tedious needs in handling and poor mass transport (Goldstein et al., 2001). Furthermore, Freed and Vunjak-Novakovic (1995) reported that spinner flasks may not be optimal because the turbulent flow and the associated higher shear stress induce the formation of an outer fibrous capsule in the cartilaginous tissue grown. Another drawback associated with the rotating wall systems is that growth of tissue is usually non-uniform (Chen and Hu, 2006; Freed and Vunjak-Novakovic, 1997). The centrifugal force does improve mass transport, but causes the scaffolds to frequently collide with the bioreactor wall. This induces cell damage and disrupts cell attachment and matrix deposition on the scaffolds (Goldstein et al., 2001). Wiesmann et al. (2004) state further limitation of spinner flasks by noting that as these bioreactor systems require individual manual handling for medium exchange, cell seeding, etc., ultimately limit their usefulness when large cell numbers are required. It is understood that sometimes one may need to operate at low cell densities (e.g. for contact inhibition, reduced proliferation rates, enhanced differentiation), but this differs from our aim to produce 3D bone tissue of clinical dimensions. We agree with Martin and Vermette's (2005) opinion that spinner flasks and rotating wall vessels are of limited use to grow large tissue mass.

It is evident from the above discussion that characterizing nutrient transport in bioreactors is critical in the effort to grow bone tissue constructs of clinical value. However, these bioreactors are generally very small in size (our HFMB is 3.0cm in length, with each hollow fiber module having a 0.4mm extracapillary space between each other) and this makes in situ monitoring of concentration distribution very difficult with current monitoring technology. Furthermore, the bioreactors operate under stringent conditions (specific cell-culture and sterile conditions, etc.). Due to these particulars, computational modelling is increasingly being used to understand the mass transport behaviour in the bioreactors and to characterize their functions at different operating conditions (Das, 2007; Abdullah and Das, 2007; Ma et al., 2007; Sengers et al., 2007; Abdullah et al., 2006; Ye et al., 2006). While there are different bioreactors, it seems there is no systematic comparison of these bioreactors to confirm the suitability / effectiveness of these bioreactors for BTE. In particular, there is a

lack of computational or experimental study to confirm the assertion that HFMB is more suitable for growing bone tissues. To address this issue, we use computational modeling to carry out a systematic comparison of three bioreactors which are expected to justify which of these bioreactors are better suited for growing bone tissues (at high cell densities). We define that the suitability of the bioreactors is governed by the need to obtain high cell density in bone tissues of clinical size. However, the comparisons of the bioreactors are made by characterizing nutrient transport for given cell density. The mathematical frameworks are presented for nutrient transport in hollow fiber membrane bioreactor (HFMB), the confined perfusion bioreactor (CPB) and the suspended tube bioreactor (STB). These bioreactors are specifically chosen to represent a sophisticated perfused type, a simple perfused type and simple culture dish/flask type bioreactors (non-perfused), respectively, in terms of their geometrical configurations.

2. Governing model equations

2.1 Hollow fiber membrane bioreactor (HFMB)

In this work, we use the Krogh cylinder approximation of HFMB for developing the numerical model. This allows us to define the HFMB as composed of many identical fibers and the same flow and transport behaviour within each fiber (Abdullah and Das, 2007; Brotherton and Chau, 1996; Labecki et al., 1996, 1995; Taylor et al., 1994; Kelsey et al., 1990; Bruining, 1989; Apelblat et al., 1974). A representative diagram of Krogh cylinder can be seen in Figure 3. The figure reveals the three main Krogh cylinder sections, namely, the lumen, membrane wall and the extracapillary space (ECS). The regions labelled R_1, R_2 and R_3 represent the radius of the fiber lumen, R_1 plus membrane wall thickness and R_2 plus the thickness of the ECS, respectively. In this work, the HFMB domain is defined as a 2-D Krogh cylinder representation in an axisymmetrical co-ordinate system, also shown in Figure 3. In the figure, segments A1, A2 and A3 represent the lumen radius, the membrane wall thickness and half of the total ECS thickness, respectively.

In order to model nutrient transport in the HFMB, steady state equations of conservation of momentum and mass are solved simultaneously. All governing equations (conservation and boundary equations) needed to simulate nutrient transport behaviour in the HFMB are defined in the following sections.

2.1.1 HFMB Lumen

We define the fluid motion in the lumen region to be incompressible and steady. The conservation of motion is governed by the equations (1) and (2) in stationary (Eulerian) co-ordinate system. Equation (1) is the Navier-Stokes (NS) equations for conservation of fluid

momentum, whilst equation (2) represents conservation of fluid mass (incompressible fluid). The boundary conditions (BCs) describe axial symmetry conditions (3a), no slip at the wall (3b), a fully developed parabolic flow profile at the entrance of the lumen (3c) and normal outlet condition (3d), respectively. In these equations, η denotes fluid dynamic viscosity (kg m^{-1} s^{-1}), $\vec{u}$ is the velocity vector (m s^{-1}), u_{avg} is the average fluid velocity, u and v are the velocity components in the axial (z) and radial (r) directions (m s^{-1}), ρ is density (kg m^{-3}) and $\vec{F}$ is the force vector (kg m s^{-2}).

Conservation of fluid momentum: $$-\eta\nabla^2\vec{u} + \rho(\vec{u}\cdot\nabla)\vec{u} + \nabla p = \vec{F} \quad (1)$$

Conservation of fluid mass: $$\nabla\cdot\vec{u} = 0 \quad (2)$$

BCs: $$\frac{\partial u}{\partial r} = \frac{\partial v}{\partial r} = 0 \text{ at } r = 0 \quad (3a)$$

$$u = v = 0 \text{ at } r = R_1 \quad (3b)$$

$$v = 2u_{avg}(1 - r^2/R_1^{\,2}),\ u = 0 \text{ at } z = 0 \quad (3c)$$

$$p = 0, \quad z = L_1 \quad (3d)$$

The equation for conservation of nutrient mass in the lumen is represented by equation (4), which is subjected to BCs as in equations (5a-d). In the fiber lumen, the nutrient transport is mainly achieved by means of axial convection and diffusion. We define that in this region (lumen), the nutrient transport velocity is the same as fluid velocity field ($\vec{u}$), determined from equations 1, 2, 3a and 3b.

Conservation of nutrient mass: $$\nabla\cdot\left(-D_1\nabla c\right) = -\vec{u}\cdot\nabla c \quad (4)$$

BCs: $$c = c_0 \text{ at } z = 0 \quad (5a)$$

$$\vec{n}\cdot\left(-D_1\nabla c + c\vec{u}\right) = \vec{n}\cdot\left(c\vec{u}\right) \text{ at } z = L_1 \quad (5b)$$

$$\frac{\partial c}{\partial r} = 0 \text{ at } r = 0 \quad (5c)$$

$$D_1\frac{\partial c}{\partial r} = D_2\frac{\partial c}{\partial r} \text{ at } r = R_1 \quad (5d)$$

As evident, four BCs are defined. The first BC (5a) is a Dirichlet type BC representing the inlet concentration at the entrance to the lumen. Equation (5b) and (5c) are Neumann type BCs corresponding to convective flow (outlet) and axial symmetry at the centre of the lumen. The fourth BC (5d) is also a Neumann type BC and accounts for the conservation of flux at the lumen wall. In the above and subsequent equations, L_1 is the effective HF length, c is concentration (mol m^{-3}), $\vec{n}$ is unit vector perpendicular to the boundary and the parameter D with subscripts 1, 2 and 3 refers to the diffusivity values of a nutrient in the lumen (A1), fiber membrane wall (A2) and cellular matrix (A3), respectively.

2.1.2 HFMB Fiber Membrane Wall

In the fiber membrane wall, we define equation (6) to represent conservation for nutrient mass with respect to equations (7a-c) as boundary equations. Equation (6) describes the nutrient conservation equation with zero fluid velocity as there is no fluid flow in the membrane. Here, we define the membrane region having no convection and nutrient transfer is via diffusion only. BC (7a) is identical to the BC (5d) in the lumen and along with (7b) accounts for the conservation of flux at the membrane boundaries with the lumen and ECS respectively. BC (7c) meanwhile accounts for insulation where nothing passes in or out of the boundary.

Conservation of nutrient mass: $$\nabla \cdot \left(-D_2 \nabla c\right) = 0 \quad (6)$$

BCs: $$D_1 \frac{\partial c}{\partial r} = D_2 \frac{\partial c}{\partial r} \text{ at } r = R_1 \quad (7a)$$

$$D_2 \frac{\partial c}{\partial r} = D_3 \frac{\partial c}{\partial r} \text{ at } r = R_2 \quad (7b)$$

$$\vec{n} \cdot \left(-D_2 \nabla c\right) = 0 \text{ at } z = 0, L_1 \quad (7c)$$

2.1.3 HFMB Extracapillary Space (ECS)

In the extracapillary space (ECS), we define equations (8a-b) to represent conservation for nutrient mass, with respect to equations (9a-c) as boundary equations.

Conservation of nutrient mass: $$\nabla \cdot \left(-D_3 \nabla c\right) = \hat{R} \quad (8a)$$

$$\hat{R} = -V \times d \quad (8b)$$

BCs: $$D_2 \frac{\partial c}{\partial r} = D_3 \frac{\partial c}{\partial r} \text{ at } r = R_2 \quad (9a)$$

$$\vec{n} \cdot \left(-D_3 \nabla c\right) = 0 \text{ at } z = 0, L_1 \quad (9b)$$

$$\frac{\partial c}{\partial r} = 0 \text{ at } r = R_3 \quad (9c)$$

Equation (8a) shows that the rate of diffusion is related to the product reaction rate, $\hat{R}$. In equation (8b), we define that reaction rate, which is also the cell nutrient consumption rate to be of zero order kinetics. By defining the reaction rate this way, we aim to show the worst case scenarios for concentration distributions (i.e., nutrient deficiencies) under different conditions. This issue was discussed in detail in our previous papers (Abdullah and Das, 2007; Abdullah et al., 2006; Ye et al., 2006). In brief, zero order kinetics was chosen because our inlet concentration used based on the manufacturer's formulation (Ye et al., 2006) is about 1000 times higher than reported values of the Michaelis-Menten constant, K_m (Ma et al., 2007). Although the most common rate expression is of Michaelis-Menten type, that rate of expression reduces to zero order kinetics at high nutrient concentrations, i.e. where K_m is

much smaller than concentration, c (Fujimiya et al., 1999; van Wensem et al., 1997; Brotherton and Chau, 1996). In the above equations, variables V and d are defined as cell metabolic rate for glucose (mol $cell^{-1}$ s^{-1}) and cell seeding density (cells m^{-3}), respectively. BC(9a) is similar to BC (5d), while BCs (9b-c) reflect containment at both ends of the ECS and the symmetry of the concentration gradients between adjacent hollow fibers respectively.

2.2 Confined perfusion bioreactor (CPB)

For the purpose of our numerical simulations, we define that the CPB is divided into three sections which are the lumen, the membrane wall and the scaffold construct. This is represented in Figure 2. Section B1, which is the lumen, is similar to the fiber lumen in the HFMB. It is through here that the nutrients and growth factors are supplied to, and wastes removed from the bioreactor. Region B2 or the membrane wall is porous and semi-permeable to certain solutes such as nutrients and oxygen. The third section, B3, represents the scaffold matrix construct which will support the bone tissue cells and allow them to grow and proliferate. Symbols R_4, R_5 and R_6 represent the scaffold boundary, membrane boundary and outer boundary of the CPB, respectively.

The governing equations associated with the CPB are comparable to those for the HFMB. It again involves the simultaneous solution of the equations for steady state conservation of momentum in the lumen region combined with the conservation of mass in all three previously defined regions. All governing equations used to simulate nutrient transport behaviour in the CPB are defined as follows.

2.2.1 CPB Lumen

As in the HFMB, the fluid motion in the lumen region of the CPB is incompressible and steady. Therefore, the same equations (1) and (2) are used to govern the conservation of momentum and mass of the fluid respectively, in the CPB. These equations are subject to the BCs as depicted by equations (10a-d). BCs (10a) and (10b) describe axial symmetry and no slip boundary conditions; BC (10c) describes a fully developed parabolic flow profile at the inlet, while BC (10d) describes the outlet. Symbol x in (10b) is the radial distance of the CPB lumen.

Conservation of fluid motion and fluid mass:
Equations (1) and (2)

BCs: $$\frac{\partial u}{\partial r} = \frac{\partial v}{\partial r} = 0 \text{ at } r = 0 \quad (10a)$$

$$u = v = 0 \text{ at } r = x, R_5, R_6 \quad (10b)$$

$$v = 2u_{avg}(1 - r^2 / x^2),\ u = 0 \text{ at } z = 0 \quad (10c)$$

$$p = 0, \quad z = L_1 \tag{10d}$$

The conservation of mass (nutrient) equations for each region and their respective BCs are almost identical to those in the HFMB. In the CPB lumen, conservation of nutrient mass is represented by equation (11), whilst equations (12a-e) represent the BCs. Symbols D_4, D_5 and D_6 are the diffusivity values of nutrient ($m^2\ s^{-1}$) in the lumen, membrane, and scaffold construct in CPB, respectively. L_2 meanwhile is the CPB effective length of CPB.

Conservation of nutrient mass: $$\nabla \cdot \left(-D_4 \nabla c\right) = -\vec{u} \cdot \nabla c \tag{11}$$

BCs: $$c = c_0 \text{ at } z = 0 \tag{12a}$$

$$\vec{n} \cdot \left(-D_4 \nabla c + c\vec{u}\right) = \vec{n} \cdot \left(c\vec{u}\right) \text{ at } z = L_2 \tag{12b}$$

$$\frac{\partial c}{\partial r} = 0 \text{ at } r = 0 \tag{12c}$$

$$\vec{n} \cdot \left(-D_4 \nabla c + c\vec{u}\right) = 0 \text{ at } r = x, R_6 \tag{12d}$$

$$D_4 \frac{\partial c}{\partial r} = D_5 \frac{\partial c}{\partial r} \text{ at } r = R_5 \tag{12e}$$

2.2.2 CPB Fiber Membrane

In the fiber membrane, conservation of mass (nutrient) is represented by equation (13), with equations (14a-c) being the BCs.

Conservation of nutrient mass: $$\nabla \cdot \left(-D_5 \nabla c\right) = 0 \tag{13}$$

BCs: $$D_4 \frac{\partial c}{\partial r} = D_5 \frac{\partial c}{\partial r} \text{ at } r = R_5 \tag{14a}$$

$$D_5 \frac{\partial c}{\partial r} = D_6 \frac{\partial c}{\partial r} \text{ at } r = R_4 \tag{14b}$$

$$\frac{\partial c}{\partial r} = 0 \text{ at } r = 0 \tag{14c}$$

2.2.3 CPB Scaffold Construct

In the scaffold construct, equations (15a-b) are defined to correspond for conservation of mass (nutrient), subjected to equations (16a-b) as boundary conditions respectively.

Conservation of nutrient mass: $$\nabla \cdot \left(-D_6 \nabla c\right) = \hat{R} \tag{15a}$$

$$\hat{R} = -V \times d \tag{15b}$$

BCs: $$D_5 \frac{\partial c}{\partial r} = D_6 \frac{\partial c}{\partial r} \text{ at } r = R_4 \tag{16a}$$

$$\frac{\partial c}{\partial r} = 0 \text{ at } r = 0 \tag{16b}$$

2.3 Suspended tube bioreactor (STB)

We define that the STB has two sections, as in Figure 1. The first section, C1, represents nutrient rich solution which is in the bioreactor vessel while the second section, C2, corresponds to suspended scaffold construct with bone tissue cells within. R_7 and R_8 are defined as radius of the flask and radius of the scaffold construct, respectively.

No flow is considered in the STB (as we introduce it as a non perfused system). We define that the medium is well mixed. Thus, the only equations for conservation of mass (nutrient) are used in the defined domains. The cylindrical geometry of the STB is set in a 2-D axisymmetrical coordinate system for the numerical simulations. The governing equations for the STB are given as follows.

2.3.1 STB Vessel

Equation 17 represents conservation of mass (nutrient) in the STB vessel, subjected to boundary conditions in equations (18a-c).

Conservation of nutrient mass: $$\nabla \cdot \left(-D_7 \nabla c\right) = 0 \quad (17)$$

BCs: $$\frac{\partial c}{\partial r} = 0 \text{ at } r = 0, \quad (18a)$$

$$\vec{n} \cdot \left(-D_7 \nabla c\right) = 0 \text{ at } r = R_7,\ z = 0,\ L_3 \quad (18b)$$

$$D_7 \frac{\partial c}{\partial r} = D_8 \frac{\partial c}{\partial r} \text{ at } r = R_8,\ z = z_1,\ z_1 + z_2 \quad (18c)$$

2.3.2 STB Scaffold Construct

In the scaffold construct, conservation of mass (nutrient) is represented by equations (19a-b). Boundary conditions for this domain are represented by equations (20a-b). Symbols D_7 and D_8 in the above mentioned equations are the diffusivity values of given nutrient species ($m^2\ s^{-1}$) in the vessel and scaffold of the STB respectively. L_3 meanwhile is the effective length of the STB, defined by the height level of nutrients in the STB vessel.

Conservation of nutrient mass: $$\nabla \cdot \left(-D_8 \nabla c\right) = \hat{R} \quad (19a)$$

$$\hat{R} = -V \times d \quad (19b)$$

BCs: $$D_7 \frac{\partial c}{\partial r} = D_8 \frac{\partial c}{\partial r} \text{ at } r = R_8,\ z = z_1,\ z_1 + z_2 \quad (20a)$$

$$\frac{\partial c}{\partial r} = 0 \text{ at } r = 0 \quad (20b)$$

2.4 Model parameters

In this work, we use constants and operational parameters which are the same as used in our previous studies (Abdullah and Das, 2007; Das, 2007; Abdullah et al., 2006; Ye et al., 2006). These are detailed in Table 1. The significant parameters of the HFMB (e.g. fiber diameter, membrane thickness etc) are referred from the same above mentioned source. As these values (Table 1) are taken directly from in-house experiments, they also reflect laboratory conditions.

The geometry of the CPB (Table 1) is chosen to give a scaffold size that would provide cell tissues of comparable size to the HFMB and so provides a good comparison between the two reactors. In Table 1, the magnitudes of the parameters in the radial direction are ten times greater in the CPB than the HFMB. The geometry of the STB is similar to the suspended tube model proposed by Sengers et al. (2005) and reflects a realistic non-perfused bioreactor.

2.5 Solving governing equations, boundary conditions and model parameters

The numerical solutions to the governing equations have been obtained using FEMLAB. When solving the governing partial differential equations (PDEs) the software applies finite element method (FEM) to discretise and solve the PDEs (FEMLAB User's Guide, 2004). FEMLAB runs the finite element analysis together with adaptive meshing and error control using a variety of iterative numerical solvers. FEMLAB generates a mesh that is tetrahedral in shape and isotropic in size. A vast number of elements can then be created with or without any scaling requirements. In our simulations for HFMB, a scaling factor of 10 has been used in the radial direction due to the significant difference in the magnitude of r (radial distance) and z (axial distance). The geometry is automatically scaled back after meshing. This generates an anisotropic mesh and the HFMB geometry has 2,202 elements with 8,726 degrees of freedom (DOF) instead of 22,125 elements and 87,133 DOF. For the CPB we use a mesh consisting of 4,278 elements and have 31,860 DOF while for the STB's geometry, 311 elements and 681 DOF are used.

We performed simulations with different mesh sizes, which are within the range of FEMLAB's predefined mesh size schemes, e.g., 'extremely course', 'extra course', 'courser', 'course', 'normal', 'fine', 'finer', 'extra fine' and 'extremely fine'. Statistics of number of element and DOF for 'extremely course', 'normal' and 'extremely fine' schemes for our HFMB Krogh cylinder framework are 1248-6401, 2202-8276 and 4722-16596, respectively. Varying the mesh schemes (using the three previously mentioned predefined mesh scheme), showed results with very small difference in concentration value when they are compared (typically <1% difference). We realize that if we continued to use coarser grids, the mesh sizes may affect the simulation results slightly. We did further simulations on our framework

(Krogh cylinder) with finer mesh scales (up to 140982 elements) and obtained small differences in the concentration profiles. We believe that this illustrates that the mesh sizes that we used for our simulations are fine enough to give converged numerical results. In order to get a good comparison between the bioreactor domains, we used the same predefined FEMLAB mesh sizes (predefined mesh scale is being set at normal) for each bioreactor.Using different mesh grids and scaling factors to descritize the defined domains may give significant effect on simulation results. In our case, as discussed by Ye et al. (2006), our current simulations give small concentration difference when meshes of 2,202 elements and 140,928 elements were compared. In order to get a good comparison, we used the same predefined FEMLAB mesh sizes (predefined mesh scale is being set at normal) for each bioreactor (each with DOFs and elements as mentioned in the previous paragraph). Small differences may be observed with addition of scaling coefficients. This is because FEMLAB automatically scales back the geometry after meshing (Ye et al., 2006).

As previously mentioned, validity of the results is difficult to obtain due to the very small laboratory scale of the bioreactors. Experiments carried out by Ye et al. (2004) found that only collective concentration change at the inlet and outlet of the bioreactor could be monitored at different time. It was not possible to monitor localised concentration data within the bioreactor. Further, the experimentally measured concentrations do not reflect what may happen at steady state conditions. This created a problem in that the results obtained from the FEM package cannot be directly compared to experimental results for model validation. However, due to the inherent nature of FEM, mass is conserved in the domain. Furthermore, the developed scheme has been validated against benchmark solutions as discussed by and Abdullah and Das (2007), Abdullah et al. (2006) and Ye et al. (2006). For brevity, they are not discussed in this paper.

3. Results and discussions

In this section, we present our simulation results for nutrient transport behaviour. It is divided into three main parts which cover the hydrodynamics and nutrient transport behaviour in all three bioreactors (HFMB, CPB and STB). In our previous papers on HFMB (Abdullah and Das, 2007; Abdullah et al., 2006; Ye et al., 2006), we have shown that at high cell densities, glucose rather than oxygen is the limiting nutrient. Consequently, only glucose concentration profiles are considered for the purpose of this paper.

In an effort to ensure that ample amounts of nutrients are available for cells to metabolize, we argue that nutrient concentration in the bioreactors are more critical in areas / domains where cells are grown (e.g., ECS) as compared to other areas (e.g., lumen). Therefore, our

concentration profile results will mainly be shown in areas where there is cell growth, i.e. the ECS in the HFMB and, the scaffold matrix in the CPB and STB. For our work, all simulations define a zero order consumption rate in continuation of our previous work. The effects of the rate of reaction have been considered in a previous work (Abdullah et al., 2006).

3.1 Fluid flow and mass transfer characteristics

In this section, we present the fluid flow and mass transfer characteristics in the HFMB, CPB and STB, respectively. These are presented in an attempt to characterize and compare the hydrodynamics in those bioreactors. We start doing so by defining three important dimensionless parameters for each bioreactor, namely, the Reynolds (Re), Peclet (Pe) and Damkohler (Da) numbers. They are defined as below:

$$\mathrm{Re} = \frac{\text{Dynamic Pressure}}{\text{Shear Stress}} \tag{21a}$$

$$\mathrm{Re}_{HF} = \frac{\rho u_{avg} L_{c\,HF}}{\eta} \tag{21b}$$

$$\mathrm{Re}_{CPB} = \frac{\rho u_{avg} L_{c\,CPB}}{\eta} \tag{21c}$$

$$\mathrm{Pe} = \frac{\text{Rate of Flow Advection}}{\text{Rate of Diffusion}} \tag{21d}$$

$$\mathrm{Pe}_{HF} = \frac{L_{cHF} u_{avg}}{D_1} \tag{21e}$$

$$\mathrm{Pe}_{CPB} = \frac{L_{cCPB} u_{avg}}{D_4} \tag{21f}$$

$$\mathrm{Da} = \frac{\text{Rate of Nutrient Intake}}{\text{Rate of Transport Advection}} \tag{21g}$$

$$\mathrm{Da}_{HF} = \frac{\mathrm{Vd}(c_0)^{n-1} A_3}{D_3} \tag{21h}$$

$$\mathrm{Da}_{CPB} = \frac{\mathrm{Vd}(c_0)^{n-1} A_6}{D_6} \tag{21i}$$

$$\mathrm{Da}_{STB} = \frac{\mathrm{Vd}(c_0)^{n-1} A_8}{D_8} \tag{21j}$$

Re and Pe numbers are only calculated in the lumen of HF and CPB, where velocity is defined. As for Da, it is only determined in HF ECS, CPB and STB scaffold construct, respectively (where reactions take place). For equations (21a-j), ρ is defined as fluid density

($kg\ m^{-3}$), u_{avg} is average fluid velocity ($m\ s^{-1}$), L_c is the characteristic length or lumen diameter (m) of CPB and the fiber module in HFMB and η is the dynamic fluid viscosity ($kg\ m^{-1}\ s^{-1}$). D with subscripts are similar to what was previously defined, n is defined as reaction order while A is defined as interfacial surface area with subscripts 3, 6 and 8 represents domains of the HF Krogh cylinder ECS and scaffold constructs of CPB and STB respectively.

We have calculated Re and through equation (21a-c). For calculation of Re, the density variation in the lumen is discarded because of a few reasons. One, the glucose concentration in the lumen is very dilute ($5.55\ mol\ m^{-3}$) and the weight of nutrients is very small compared to water to be giving effective variation on overall density. Secondly, the temperature and pressure is kept constant and any variations of these parameters inside the bioreactors are too small to influence the overall fluid density. Due to this, it is safe enough to estimate the fluid properties using water properties at 310K (37^oC). From above equations (21b-c), the Reynolds number in the HF module in HFMB is 2.138 while Re in CPB is 21.38. Both values imply laminar flow ($Re << 2100$). Re values also shows that inertial forces in the HFMB and CPB are 2.138 and 21.38 times higher than the viscous forces. Viscous forces in the HF module and CPB are defined to be the same, but CPB has inertia forces 10 times larger than a single HF module. This is because CPB has an L_c value of 10 times larger, when all other operational parameters (ρ, u and μ) are the same.

As for Pe values obtained from equation (21d-f), it is revealed that Pe in HFMB is at 2759.26 while CPB is 10 times higher at 27592.6. This implies that rate of flow advection in an HF module and CBP lumens are 2759 and 27592 times higher than the rate of diffusion respectively. It is obvious that CPB has a Pe 10 times higher than HFMB, due to similar reasons explained in the previous paragraph. The bioreactor is operating in a convective dominant regime when $Pe >> 1$. Hence, in the lumen, solute transport is achieved by convection.

The Da values for zero order kinetics and with similar operating conditions, are 28.91 for an HF module in HFMB, 32.11 for CPB and 321.18 for STB, from equation 21(g-j). This implies that under the specified conditions for all three bioreactors, the chemical reaction rate (nutrient uptake by the cells) is high compared to mass transport rate. In other words, these bioreactors are diffusion limited when $Da >> 1$ (Gervais and Jensen, 2006; Mousavi et al., 1999).

3.1.1 Hollow fiber membrane bioreactor (HFMB)

Under the control parameters (Table 1), the simulated fluid flow and mass transfer characteristics of the HFMB can be seen in Figures 4(a-d). Figure 4(a) shows the magnitude of fluid velocity field in the HFMB lumen. As expected, the flow profile in the lumen is parabolic. Figure 4(b) shows that the diffusive flux in the membrane and ECS regions is in the radial direction. This is expected as the concentration gradient is in the radial direction and the nutrients diffuse along the same direction of concentration gradient according to the governing equations. Figures 4(c,d) show that the inlet of the HFMB is at a higher pressure while the outlet is at zero (gauge) pressure, similar to the profiles produced by Brotherton and Chau (1996). It is this pressure gradient that drives the fluid through the lumen region.

3.1.2 Confined perfusion bioreactor (CPB)

The simulated fluid flow and mass transfer characteristics in the confined perfusion bioreactor for control parameters are shown in Figures 5(a-d). It can be seen in Figure 5(a) that the flow profiles in the CPB are parabolic although the fluid velocity is low around the middle of the reactor. Figures 5(b,c) show that the diffusive flux in the membrane and ECS regions is in the radial direction towards the centre of the bioreactor. This conforms to what is expected from the governing equations. Figure 5(d) meanwhile shows the pressure gradient that drives the flow through the lumen region.

3.1.3 Suspended tube bioreactor (STB)

The mass transfer characteristics for the simulation of the confined perfusion bioreactor operating for control parameters can be seen in Figure 6. There is no fluid flow profile associated with the STB. Figure 6 shows that the mass transfer processes in the STB are dominated by diffusive mechanisms. The magnitude of the flux is seen the greatest close to the scaffold.

3.2 Nutrient concentration profiles

The results discussed in this section are for the parameter values in Table 1, which reflect in-house laboratory experiments (Abdullah et al., 2006; Ye et al., 2006).

3.2.1 Hollow fiber membrane bioreactor (HFMB)

The axial and radial concentration profiles for glucose in the HFMB are shown in Figure 7. The figure shows that glucose concentration is available to maintain cell growth throughout the ECS domain (under controlled conditions). It can be seen that the axial variation of glucose concentration is very small while its radial profile shows a greater drop in concentration towards the outer radius of the hollow fiber. Radial concentration variations are larger because increasing radial distance is effectively moving further away form the nutrient

source. Furthermore, the radial nutrient transport depends on diffusion mechanism through the membrane wall and ECS. The lateral changes in concentration are consistent with the HFMB behaviour predicted earlier and were reported by various researchers, among others, Abdullah and Das (2007), Brotherton and Chau (1996) and Heath and Belfort (1987).

3.2.2 Confined perfusion bioreactor (CPB)

The axial and radial glucose concentration profiles in the CPB are shown in Figure 8. The figure shows that glucose concentration in the CBP decreases towards the centre of the scaffold. Similarly to the HF Krogh cylinder, the CPB scaffold centre has the lowest nutrient concentration because it is furthest from the nutrient source. Again, nutrient transport is fully dependent on diffusion mechanisms alone to allow glucose to be delivered to the centre. The axial profile is seen symmetric because the defined diffusion coefficient and nutrient uptake rate (reaction rate) are kept constant throughout the scaffold. The scaffold centre has the lowest nutrient concentration because it is furthest from the nutrient source. Furthermore, it is fully dependent on diffusion mechanisms alone to allow glucose to be transported to the area. The scaffold centre of the CBP is left with only ≈10% of the inlet glucose concentration (c_0). This glucose concentration is unlikely to sustain cell growth. The profiles obtained here are similar to what were reported by Sengers et al. (2005).

3.2.3 Suspended tube bioreactor (STB)

The axial and radial glucose concentration profiles in the STB are shown in Figure 9. The negative concentration values imply the amount of nutrients that are deprived from the cells in the scaffold domain. The figure suggests that glucose concentration is severely inadequate to maintain cell growth in the scaffold domain. Such glucose deficiency will ultimately lead to cell death. This implies that the STB may not be a feasible bioreactor for growing high cell density bone tissues. The profiles showed here are somewhat of similar trend to what were discussed by Sengers et al. (2005). In our work, we have the same cell density in the CPB and HFMB to make a direct comparison possible.

3.3 Effects of process design parameters

The glucose concentration profiles presented in this section are from further simulations that are carried out by varying a parameter of interest, whilst keeping the other parameters the same. By comparing the profiles obtained from the variations of chosen parameters against the control cases, the manifestation of various parameters on nutrient transport behaviour in each bioreactor are determined. There are a number of design parameters affecting the mass transfer characteristics of the bioreactors. In this section, the effects of inlet glucose concentration (c_0), inlet velocity (u), cell density (d) and hindering factor (β) on nutrient

concentration profiles are observed. The reasons why these parameters are chosen are explained in the sections to follow. In this section, concentration profiles in the HFMB are represented by only radial profiles, whilst the CBP and STB will be represented by axial profiles only. We have decided to choose these profiles because more significant transport limitations are shown radially in the HFMB (as opposed to axially in the said bioreactor) and axially in both CPB and STB (as opposed to radially in both) under control conditions.

3.3.1 Effect of inlet glucose concentration (c_0)

The inlet concentration of nutrients is an important parameter in the design of a bioreactor and it is important to understand how change of inlet glucose concentration (c_0) influences the mass transfer behaviour in the bioreactors. The previous simulations in this paper have been carried out for inlet concentration of 5.55 mol m^{-3}, which reflects the laboratory scale experiments (Ye et al., 2006). In this section, we have simulated bioreactor operations with different nutrient inlet concentrations. This is done with the aim to observe whether glucose transfer limitations observed under control conditions can be sufficiently reduced by varying inlet concentrations. This corresponds to a logical and direct answer/solution for nutrient deficiency, which is to increase the supply of nutrients. With slight note of caution, it must be pointed out that it is important to understand that cell deaths are not only related to lack of nutrients. It is also possible to kill cells by supplying them with too high concentrations of nutrient. Furthermore, supplying too much nutrient may not be the best solution in terms of cost and maintenance. The ranges of glucose concentrations have been continued from those chosen by Abdullah and Das (2007), Das (2007), Abdullah et al. (2006) and Ye et al. (2006). The effects of inlet glucose concentrations are shown in Figures 10 and 11 for HFMB, and CPB respectively.

In general, these figures show that increasing c_0 values leads to higher nutrient availability in the extracellular regions. Figures 10 and 11 show that increasing the glucose inlet concentration in the HFMB and CPB produce elevated concentration profiles (higher concentration values). For example, the lowest point of c/c_0 in the CPB increases from 0.1 (for glucose inlet concentrations of 5.55 mol m^{-3}) to $c/c_0 \approx 0.41$ (for inlet concentrations of 8.50 mol m^{-3}). This improvement enhances the possibility of the CPB to sustain growth of cells at high densities, which is crucial in producing clinically viable bone tissue constructs. However, the large variation in glucose concentration (high glucose concentration gradient) observed in the CPB as in Figure 11 may lead to an uneven distribution and density of cells. In the STB, increasing inlet glucose concentration even up to 8.50 mol m^{-3}, fails to significantly improve transport limitations in the scaffold construct. Without ample nutrient supply, it seems that the STB is unsuited for growth of cells at high density. The STB

concentration profiles are similar to Figure 9 and are below zero for all different inlet concentrations. Thus, the STB profiles are not shown.

From these simulations, we show that glucose concentration profiles are affected by inlet concentrations. It is also shown that nutrient transport limitation can be significantly reduced, although not completely removed by increasing nutrient inlet concentrations (c_0). Nonetheless, increasing the inlet glucose concentration does not overly improve the performance of HFMB, which implies that an inlet concentration of 5.55 mol m^{-3} is ample for operations at a high cell density (e.g. 2×10^{12} cells m^{-3}). For CPB, the inlet concentration may need to be increased to levels high enough to sustain cell growth at these cell densities (2×10^{12} cells m^{-3}). For STB however, increasing inlet glucose concentrations alone is not enough to ensure feasibility in growing cells at high density. With slight note of caution, one should note that in good condition, the cell number in the ECS or scaffolding matrix should increase in time. It may be wise to increase the inlet concentration once cells increase in number (cell density increases) in order to maintain similar concentration profiles throughout the ECS or scaffolding matrix. The effects of cell density on concentration profiles throughout each bioreactor are shown in section 3.3.3 in this paper.

3.3.2 Effect of fluid inlet velocity (u_{avg})

These simulations involve observing effects of fluid inlet velocity (u_{avg}) on nutrient concentration. They only apply to the HFMB and CPB due to the fact that no fluid flow occurs in the STB. The parabolic flow profile is the same for both bioreactors with only the magnitude of u_{avg} changed. The control simulations are carried out at $u_{avg} = 7.45\times10^{-3}$ m s^{-1}. Here, we aim to investigate the effects of faster and slower fluid flow on nutrient transport. We choose velocities which are ten times greater and smaller than the control conditions. The results of these simulations are shown in Figures 12 and 13 for HFMB and CPB respectively.

It is interesting to note how differently the inlet velocity changes the glucose concentration profiles of the two bioreactors. Figure 12 shows that increasing velocity tenfold has negligible effect on glucose concentration profiles in the HFMB. However, decreasing velocity tenfold (reduced velocity of 7.45×10^{-4} ms^{-1}) display a significant effect. We may conclude here that the control velocity is the optimum velocity to be operated at cell density of 2×10^{12} cells m^{-3}. Glucose concentration profiles in the HFMB are found to be lower, especially at the furthest end of the HFMB when operated at the reduced velocity. Unlike the HFMB, inlet velocity shows little effect on glucose concentration profiles in the CPB (Figure 13). The glucose concentration profiles in the CPB show minute changes at both elevated and reduced velocity compared to profiles for control fluid inlet velocity. This means that the optimum velocity for

CPB is achieved at a reduced average velocity of 7.45×10^{-4} ms^{-1}. Operating at further reduced velocities may result in poor nutrient transport, while further increasing the velocity will not improve nutrient transport significantly.

It should be noted that the HFMB's performance is most affected by reducing the inlet flow velocity lower than control conditions. However, the concentration profile in the HFMB at reduced inlet velocities is relatively high and still adequate enough to maintain cell growth. Further simulations under even slower velocities could be carried out to see at what velocity mass transfer becomes limited to the extent of being unable to sustain the cell culture. Increasing inlet flow velocity meanwhile will result in an improved (higher) concentration profile throughout the HFMB ECS. However, this is only true up to a certain limiting value of velocity. Negligible gains in concentration are achieved if further velocity increment is made beyond the said limit (beyond control velocity). As for the CPB, inlet velocity has very small effect on its nutrient concentration profiles.

3.3.3 Effect of cell density (d)

The determination of the effects of cell density on mass transfer in the bioreactors is important. This is because it helps to identify what bone cell densities may be obtained in the bioreactors and/or the optimal operating conditions for desired cell densities. In our case, operations at high cell densities are desirable as high cell densities give higher chance to produce tissues of clinically viable size. The results of the simulations for glucose concentration profiles are shown in Figures 14 and 15 for HFMB and CPB respectively.

In general, higher cell densities result in greater nutrient consumption. For the HFMB, it can be observed from Figure 14 that lower glucose concentration profiles are exhibited at higher cell densities (up to 3×10^{12} cells m^{-3}). However, the concentration profile difference is slight, and even at an increased cell density of 3×10^{12} cells m^{-3}, more than 90% of the initial glucose concentration (c_0) is still available. This is expected to sustain further cell growth. The results obtained here correspond with earlier claims by Ye et al. (2006, 2004), Heath and Belfort (1987), that HFMB may maintain high nutrient concentrations even at high cell densities.

Meanwhile, Figure 15, which depicts axial glucose concentration profiles in the CPB, shows that the bioreactor is not able to cope with cell densities higher than 2×10^{12} cells m^{-3}. As seen in the figure, the glucose concentration profile at cell density of 3×10^{12} cells m^{-3} exhibits critical insufficiency (i.e., below zero concentration values). However, the CPB is able to maintain high concentrations of glucose at lower cell densities.

Axial glucose profiles at three different cell densities for the STB show severe insufficiency. Even small concentrations of glucose cannot be maintained throughout the scaffold construct in the STB. Glucose is seriously insufficient, even at the lowest simulated cell density (7×10^{11} cells m^{-3}). It seems that the STB may not be used for cell densities up to 7×10^{11} cells m^{-3}, although it may be used for BTE applications at lower cell densities. As all the concentration values within the STB are below zero (comparable to Figure 9), the profiles are not shown.

Increasing the cell density will increase mass transfer limitations in all three bioreactors. When designing bioreactors, it is important to determine the maximum cell densities achievable and adapt the operating conditions to achieve the desired density. From our simulations, we have shown that the STB is unsuited even at relatively low cell densities of 7×10^{11} cells m^{-3}. We have also illustrated that the CPB may not be feasible at cell densities above 2×10^{12} cells m^{-3} while the HFMB is very much capable of sustaining cell densities even at 3×10^{12} cells m^{-3}.

3.3.4 Effect of scaffold hindering factor (β)

We define hindering factors as the ratio of diffusivity of a substrate in water to its effective diffusivity in another medium. The membrane hindering factor (α) and scaffold hindering factor (β) are defined in Table 1. Hindering factors of membrane may vary due to difference in material properties (e.g. different pore sizes, tortuosity etc.). In a previous work, α was assumed to be 10 by Waterland et al. (1974) in their theoretical model for enzymatic catalysis using asymmetric hollow fiber membranes. Davis and Watson (1985) also reported an α value of 10 in their work. Others reported α values for glucose include 15 in dialysis membranes at 12 kD MWCO (molecular weight cut-off) (Myung et al., 2006) and 34 for regenerated cellulose at 3.5 kD MWCO (Marucci et al., 2007). Trujillo (1987) meanwhile, using nylon membrane, reported an α value of around 50 for uric acid. It is very unlikely that membrane with such a large hindering factor will be used for tissue engineering purposes. Our study relates to cellulose acetate HF modules with 10kDa MWCO. In the following simulations, we define a constant value of the membrane hindering factor (α) of 10. However, values for the scaffold hindering factors are not necessarily known with certainty and are often based on experimental results. Thus, variations for β will be simulated in this section. In actual practise, variations of β may represent different scaffolding materials, or conditions when diffusion coefficient decreases after time (e.g. once bone matrix grows, the effective diffusion coefficient values in the scaffold construct decreases and thus makes β values higher). Due to its high porosity (up to 90% in some cases), β value is estimated initially to be half of α, which is 5 (Willaert et al., 1999). Concentration profiles in HFMB and CPB with different β values are shown in Figures 16 and 17, respectively.

The simulations carried out under varying hindering factors (β) exhibit similar trends to simulations carried out under varying cell densities. Higher β values resulted in lower concentration levels. Nonetheless, the HFMB is able to maintain significantly high glucose concentration profiles (Figure 16) even at increased hindering factor values.

Figure 17 shows the concentration profile of glucose in the CPB respectively. From that figure, it is evident that the CPB is unable to sustain ample concentrations of glucose at increased β values. As for the STB, simulation results suggest severe glucose insufficiency with concentration values being below zero (results not shown). The severity is evident even at lower membrane hindrance factor values, thus it further reflects that the STB may not be suitable to operate under our proposed operating conditions.

4. Conclusion

A systematic comparison of three bioreactors, namely, the hollow fiber membrane bioreactor (HFMB), the confined perfusion bioreactor (CPB) and the suspended tube bioreactor (STB), has been carried out in this work using numerical experiments. It is clear that the HFMB is the most effective bioreactor for growing bulky (3-D) bone tissue. Under no operating conditions does the STB look a feasible bioreactor and it is generally hampered by mass transfer limitations. Coupled with the lack of mechanism for removing waste products, it is possible that the STB cannot be utilised to grow bone tissues under the operating conditions (especially at high cell densities) used in this work. While the CPB does not perform as well as the HFMB, it does have the potential to develop into a design capable of growing bulky bone tissues. Further tests should be carried out with a smaller scaffold domain to determine if the glucose transport limitations can be overcome. With the nutrient supply entering the bioreactor in the radial direction, it would be possible in theory to have a very long bioreactor capable of growing tissues on a larger scale than possible in the HFMB. However, the HFMB holds a significant advantage over all kinds of bioreactors, in that when the bones are implanted into the human body, the existing hollow fibers could form a capillary network allowing the transplanted bones to survive *in vivo*.

In this paper, we have showed that the HFMB is potentially a good choice in order to grow 3D bone tissue constructs. Our simulation results showed that the HFMB is able to maintain higher nutrient concentrations compared to the STB and CBP during operation. Furthermore, the HFMB performs well even at high cell densities, unlike the STB (which is unsuited at all at high densities) and the CPB (which gave mixed results at high cell densities). By varying the HFMB operational parameters, better mass (nutrient) transport can be achieved and

substantially a high nutrient concentration profile can be maintained. This reemphasises the fact that the HFMB has indeed the qualities to produce 3D bone tissue constructs of clinical value.

Acknowledgments

NSA wishes to thank the Government of Malaysia for financial support, provided through Universiti Sains Malaysia. Comments of three anonymous referees which helped to improve the clarity of the paper are also acknowledged.

Nomenclature

Symbol	Description	Units
C	concentration	mol m^{-3}
c_0	inlet glucose concentration	mol m^{-3}
D	cell density	cells m^{-3}
D	diffusion coefficient	$m^2 s^{-1}$
D_1	diffusivity in HFMB lumen	$m^2 s^{-1}$
D_2	diffusivity in HFMB membrane wall	$m^2 s^{-1}$
D_3	diffusivity in HFMB extracapillary space (ECS)	$m^2 s^{-1}$
D_4	diffusivity in CPB lumen	$m^2 s^{-1}$
D_5	diffusivity in CPB membrane wall	$m^2 s^{-1}$
D_6	diffusivity in CPB scaffold construct	$m^2 s^{-1}$
D_7	diffusivity in STB vessel	$m^2 s^{-1}$
D_8	diffusivity in STB scaffold construct	$m^2 s^{-1}$
L_c	characteristic length	m
L_1	effective fiber length	m
L_2	effective CPB length	m
L_3	effective STB length	m
n	reaction order	-
$\vec{n}$	unit vector perpendicular to the boundary	-
r	radial distance	m
$\hat{R}$	reaction term (zero order, in this paper)	dimensionless
R_1	fiber inner radius	m
R_2	fiber outer radius	m
R_3	Krogh cylinder radius	m
R_4	CPB scaffold construct radius	m
R_5	CPB membrane radius	m
R_6	CPB outer boundary radius	m
R_7	radius of STB vessel	m
R_8	radius of STB scaffold construct	m
Re	Reynolds number	dimensionless
u	velocity component in axial (x) direction	m s^{-1}
$\vec{u}$	fluid velocity field	m s^{-1}
u_{avg}	fluid average velocity	m s^{-1}
v	velocity component in radial (r) direction	m s^{-1}
V	cell metabolic rate for glucose	mol $cell^{-1}$ s^{-1}
x	radial distance of CPB lumen thickness	m
z	axial distance	m
z_1	scaffold bottom to the STB vessel bottom distance	m
z_2	thickness of STB scaffold construct	m
Greek Letters		
α	hindrance factor in membrane wall	dimensionless
β	hindrance factor in extracapillary space (ECS)	dimensionless
η	fluid dynamic viscosity	kg m^{-1} s^{-1}
ρ	fluid density	kg m^{-3}

Abbreviations

BC	boundary condition	-
BTE	bone tissue engineering	-
CPB	confined perfused bioreactor	-
DOF	degree of freedom	-
ECS	extracapillary space	-
FEM	finite element method	-
HF	hollow fiber	-
HFMB	hollow fiber membrane bioreactor	-
NS	Navier-Stokes	-
PDE	partial differential equation	-
STB	suspended tube bioreactor	-

References

Abdullah, N.S., Das, D.B., 2007. Modelling nutrient transport in hollow fiber membrane bioreactor for growing bone tissue with consideration of multi-component interactions. Chemical Engineering Science 62(21), 5821-5839.

Abdullah, N.S., Das, D.B., 2006. The hydrodynamics and molecular interaction effects on mass transfer behaviour in hollow-fiber membrane bioreactors for growing 3D bone tissue. Cytotherapy 8(2), 34.

Abdullah, N.S., Das, D.B., Ye, H. Cui, Z.F., 2006. 3D bone tissue growth in hollow fiber membrane bioreactor: Implications of various process parameters on tissue nutrition. International Journal of Artificial Organs 29, 841-851.

Apelblat, A., Katzir-Katchalsky, A., Silberberg, A., 1974. A mathematical analysis of capillary tissue fluid exchange. Biorheology 11(1), 1-49.

Brotherton, J.D., Chau, P.C., 1996. Modelling of axial-flow hollow fiber cell culture bioreactors. Biotechnology Progress 12, 575-590.

Bruining, W.J., 1989. A general description of flows and pressures in hollow fiber membrane modules. Chemical Engineering Science 44(6), 1441-1447.

Cancedda, R., Dozin, B., Giannoni, P., Quarto, R., 2003. Tissue engineering and cell therapy of cartilage and bone. Matrix Biology 22(1), 81-91.

Carrier, R.L., Papadaki, M., Rupnick, M., Schoen, F.J., Bursac, N., Langer, R., Freed, L.E., Vunjak-Novakovic, G., 1999. Cardiac tissue engineering: cell seeding, cultivation parameters, and tissue construct characterization. Biotechnology and Bioengineering 64, 580–589.

Chen, H.C., Hu, Y.C., 2006. Bioreactors for tissue engineering. Biotechnology Letters 28(18), 1415-1423.

Chong, A.K.S., Chang, J., 2006. Tissue engineering for the hand surgeon: A clinical perspective. The Journal of Hand Surgery, 31A(3), 349-358.

Cortesini, R., 2005. Stem cells, tissue engineering and organogenesis in transplantation. Transplant Immunology 15(2), 81-89.

Das, D.B., 2007. Multiscale simulation of nutrient transport in hollow fiber membrane bioreactor for growing bone tissue: Sub-cellular scale and beyond. Chemical Engineering Science 62, 3627-3639.

Davis, M.E., Watson, L.T., 1985. Analysis of a diffusion-limited hollow fiber reactor for the measurement of effective substrate diffusivities. Biotechnology and Bioengineering 27(2), 182-186.

Detamore, M.S., Athanasiou, K.A., 2005. Use of a rotating bioreactor toward tissue engineering the temporomandibular joint disc. Tissue Engineering 1, 1188–1197.

FEMLAB User's Guide, 2004. Comsol AB.

Fleming, J.E., Cornell, C.N., Muschler, G.F., 2000. Bone cells and matrices in orthopedic tissue engineering. Orthopedic Clinics of North America 31, 357-374.

Freed, L.E., Vunjak-Novakovic, G., 1998. Culture of organized cell communities. Advanced Drug Delivery Reviews 33(1-2), 15-30.

Freed, L.E., Vunjak-Novakovic, G., 1997. Microgravity tissue engineering. In Vitro Cellular and Developmental Biology-Animal 33(5), 381-385.

Freed L.E., Vunjak-Novakovic G., 1995. Cultivation of cell polymer tissue constructs in simulated microgravity. Biotechnology and Bioengineering 46, 306–313.

Freshney, R., 2000. Culture of animal cells-A manual of basic technique, 4th ed. Wiley-Liss, New York.

Fujimiya, T., Li, Y.J., Uemura, K., Ohbora, Y., 1999. Michaelis-Menten elimination kinetics of acetate in rabbit. Alcoholism: Clinical and Experimental Research 23(9), 1452-1456.

Gervais, T., Jensen, K.F., 2006. Mass transport and surface reactions in microfluidic systems. Chemical Engineering Science 61, 1102-1121.

Goldstein, A.S., Juarez, T.M., Helmke, C.D., Gustin, M.C., Mikos, A.G., 2001. Effect of convection on osteoblastic cell growth and function in biodegradable polymer foam scaffolds. Biomaterials 22, 1279–1288.

Gooch, K.J., Kwon, J.H., Blunk, T., Langer, R., Freed, L.E., Vunjak-Novakovic, G., 2001. Effects of mixing intensity on tissue-engineered cartilage. Biotechnology and Bioengineering 72, 402–407.

Heath, C., Belfort, G., 1987. Immobilization of suspended mammalian cells: analysis of hollow fiber and microcapsule bioreactors. Advanced Biochemical Engineering and Biotechnology 34, 1.

Hillsley, M.V., Frangos, J.A., 1994. Review: bone tissue engineering: the role of interstitial fluid flow. Biotechnology and Bioengineering 43(7), 573-581.

Hollinger, J.O., Einhorn, T.A., Doll, B.A., Sfeir, C., 2005. Bone Tissue Engineering. CRC Press, Florida.

Kelsey, L.J., Pillarella, M.R., Zydney, A.L., 1990. Theoretical analysis of convective flow profiles in a hollow-fiber membrane bioreactor. Chemical Engineering Science 45(11), 3211-3220.

Labecki, M., Bowen, B.D., Piret, J.M., 1996. Two-dimensional analysis of protein transport in the extracapillary space of hollow-fiber bioreactors. Chemical Engineering Science 51(17), 4197-4213.

Labecki, M., Piret, J.M., Bowen, B.D., 1995. Two-dimensional analysis of fluid flow in hollow fiber modules. Chemical Engineering Science 50(21), 3369-3384.

Lanza, R., Langer, R., Vacanti J.P., 1997. Principles of tissue engineering 2nd ed. Academic Press, New York.

Ma, C.Y.J., Kumar, R., Xu, X.Y., Mantalaris, A., 2007. A combined fluid dynamics, mass transport and cell growth model for a three-dimensional perfused bioreactor for tissue engineering of haematopoietic cells. Biochemical Engineering Journal 35(1), 1-11.

Martin, Y., Vermette, P., 2005. Bioreactors for tissue mass culture: Design, characterization, and recent advances. Biomaterials 26(35), 7481-7503.

Marucci, M., Pattersson S.G., Ragnarsson, G., Axelsson, A., 2007. Determination of a diffusion coefficient in a membrane by electronic speckle pattern interferometry: a new method and a temperature sensitivity study. Journal of Physics D: Applied Physics 40, 2870-2880.

Meyer, U., Joos, U., Wiesmann, H.P., 2004a. Biological and biophysical principles in extracorporal bone tissue engineering: Part I. International Journal of Oral and Maxillofacial Surgery 33(4), 325-332.

Meyer, U., Joos, U., Wiesmann, H.P., 2004b. Biological and biophysical principles in extracorporal bone tissue engineering: Part III. International Journal of Oral and Maxillofacial Surgery 33(7), 635 -641.

Mousavi M., Soltanieh, M., Badakhshan, A., 1999. Influence of turbulence and atmospheric chemistry on grid size with respect to location in modeling and simulation of photochemical smog formation and transport. Environmental Modelling and Software 14, 657-663.

Myung, D., Derr, K., Huie, P., Noolandi, J., Ta, K.P., Ta, C.N., 2006. Glucose permeability of human, bovine and porcine corneas in vitro. Ophthalmic Research 38(3), 158-163.

Nerem, R.M., 2006. Tissue engineering: The hope, the hype and the future. Tissue Engineering 12(5), 1143-1150.

Qiu, Q.Q., Ducheyne, P., Ayaswamy, P.S., 1999. Fabrication, characterization and evaluation of bioceramic hollow microspheres used as microcarriers for 3-D bone tissue formation in rotating bioreactors. Biomaterials 20, 989–1001.

Rose, F.R.A.J., Oreffo, R.O.C., 2002. Bone Tissue Engineering: Hope vs Hype. Biochemical and Biophysical Research Communications 292(1), 1-7.

Sengers, B.G., Taylor, M., Please, C.P., Oreffo, R.O.C., 2007. Computational modeling of cell spreading and tissue regeneration in porous scaffolds. Biomaterials 28(10), 1926-1940.

Sengers, B.G., van Donkelaar, C.C., Oomens, C.W.J., Baaijens, F.P.T., 2005. Computational study of culture conditions and nutrient supply in cartilage tissue engineering. Biotechnology Progress 21, 1252-1261.

Smalt, R., Mitchell, F.T., Howard, R.L., Chambers, T.J., 1997. Induction of NO and prostaglandin E2 in osteoblasts by wall-shear stress but not mechanical strain. American Journal of Physiology 273, 751–758.

Taylor, D.G., Piret, J.M., Bowen B.D., 1994. Protein polarization in isotropic membrane hollow fiber bioreactors. A.I.Ch.E. Journal 40(2), 321-333.

Trujillo, E.M., 1987. Transient response of encapsulated enzymes in hollow-fiber reactor. Biotechnology and Bioengineering 29(4), 529-543.

Vance, J., Galley, S., Liu, D.F., Donahue, S.W., 2005. Mechanical Stimulation of MC3T3 Osteoblastic Cells in a Bone Tissue-Engineering Bioreactor Enhances Prostaglandin E_2 Release. Tissue Engineering 11, 1832-1839.

Vunjak-Novakovic, G., Obradovic, B., Martin, I., Bursac, P., Langer, R., Freed, L., 1998. Dynamic cell seeding of polymer scaffolds for cartilage tissue engineering. Biotechnology Progress 14, 193–202.

van Wensem, J., van Straalen, N.M., Kooijman, S.A.L.M., 1997. Carbon and nitrogen fluxes in decomposing leaf litter with microbial-detritivore interactions: model simulations compare to microcosm ecotoxicity tests. Ecological Modelling 96, 175-189.

Waterland, L.R., Michaels, A.S., Robertson, C.R., 1974. A theoretical model for enzymatic catalysis using asymmetric hollow fiber membranes, AIChE J. 20, 50-59.

Wiedmann-Al-Ahmad, M., Gutwald, R., Lauer, G., Hubner., U., Schmelzeisen, R., 2002. How to optimize seeding and culturing of human osteoblast-like cells on various biomaterials. Biomaterials 23(16), 3319–3328.

Wiesmann, H.P., Joos, U., Meyer, U., 2004. Biological and biophysical principles in extracorporal bone tissue engineering: Part II. International Journal Oral and Maxillofacial Surgery 33(6), 523-530.

Wiesmann, H.P., Tkotz, T., Joos, U., Zierold, K., Stratmann, U., Szuwart T., Plate, U., Hohling, H.J., 1997. Magnesium in newly formed dentin mineral of rat incisor. Journal of Bone Mineralization Research 12(3), 380–383.

Willaert, R., Smets A., De Vuyst, L., 1999. Mass transfer limitations in diffusion-limited isotropic hollow fiber bioreactors, Biotechnology Techniques 13(5) 317-323.

Yaszemski, M.J., Payne, R.G., Hayes, W.C., Langer, R., Mikos, A.G., 1996. Evolution of bone transplantation: molecular, cellular and tissue strategies to engineer human bone. Biomaterials 17(2), 175-185.

Ye, H., Das, D.B., Triffitt, J.T., Cui, Z., 2006. Modelling nutrient transport in hollow fiber membrane bioreactors for growing three-dimensional bone tissue**.** Journal of Membrane Science 272(1-2), 169-178.

Ye, H., Xia, Z., Ferguson, D.J.P., Triffitt, J.T., Cui, Z., 2004. Hollow fiber membrane bioreactors for 3D tissue generation. Cytotherapy 6, 276.

Tables

Table 1-Operating parameters used for simulation of nutrient transport behaviour in hollow fiber membrane bioreactor (HFMB), confined perfused bioreactor (CPB) and suspended tube bioreactor (STB).

Parameter		**Symbol**	**Unit**	**Value**	**References**
Glucose diffusivity	HFMB lumen CPB lumen STB vessel	D_1 D_4 D_7	$m^2\ s^{-1}$	5.4×10^{-10}	Abdullah et al. (2006); Abdullah and Das (2007); Ye et al. (2006)
Hindering factors	Membrane	$\alpha_{HFMB} = D_1/D_2$ $\alpha_{CPB} = D_4/D_5$	-	10	
	ECS	$\beta_{HFMB} = D_1/D_3$ $\beta_{CPB} = D_4/D_6$ $\beta_{STB} = D_7/D_8$	-	5	
Medium flowrate for HFMB and CPB		u	$m\ s^{-1}$	7.45×10^{-3}	
Cell seeding density		d	cells m^{-3}	2×10^{12}	
Cell metabolic rate for glucose		V	mol $cell^{-1}$	3.83×10^{-16}	
Inlet glucose concentration for HFMB and CPB / Glucose concentration in STB vessel		c_0	mol m^{-3}	5.55	
Domain dimensions	Krogh cylinder in HFMB (Figure 3)	L_1	m	0.03	
		R_1		1.0×10^{-4}	
		R_2		1.2×10^{-4}	
		R_3		3.2×10^{-4}	
	CPB (Figure 2)	L_2		0.01	-
		x		1.0×10^{-3}	
		R_4		2.0×10^{-3}	
		R_5		2.02×10^{-3}	
		R_6		3.02×10^{-3}	
	STB (Figure 1)	L_3		0.0326	Sengers et al. (2005)
		R_7		0.01	
		R_8		5.0×10^{-3}	
		z_1		0.0148	
		z_2		3.0×10^{-3}	
Water density at 310K		ρ	kg m^{-3}	993.37	Ma et al. (2007)
Water dynamic fluid viscosity at 310K		μ	kg $m^{-1}\ s^{-1}$	0.000692	

Figures

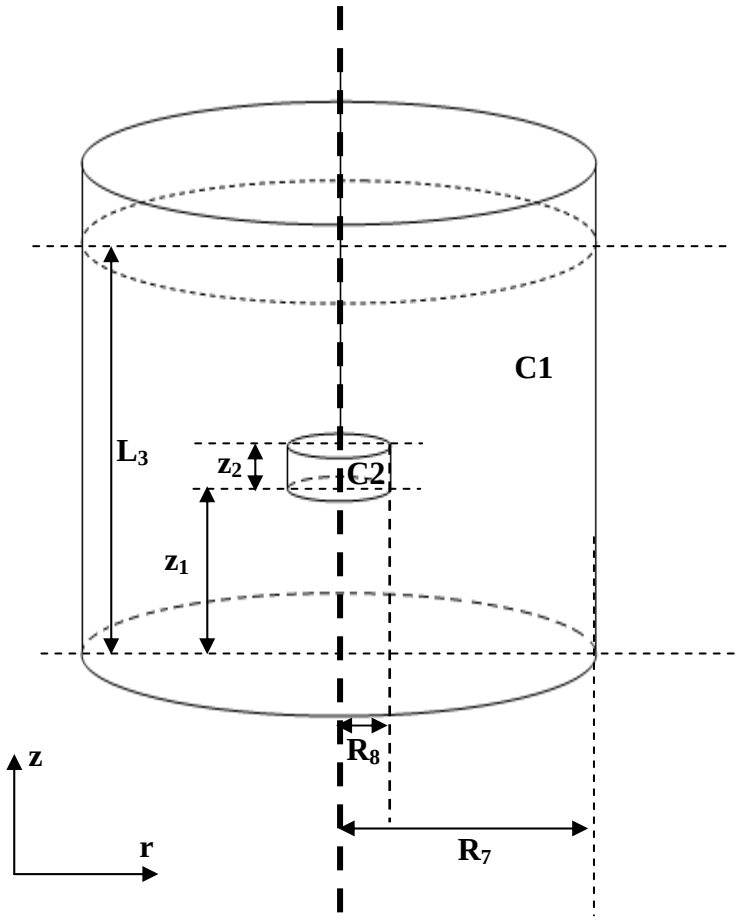

Figure 1- Schematic diagram of the suspended tube bioreactor (STB) is on the left. On the right are domains defined for nutrient transport modelling in suspended tube bioreactor. The defined domains are C1- nutrient solution which is placed in the bioreactor vessel and C2- suspended scaffold construct (with bone cells) respectively. Please refer Table 1 for dimensions.

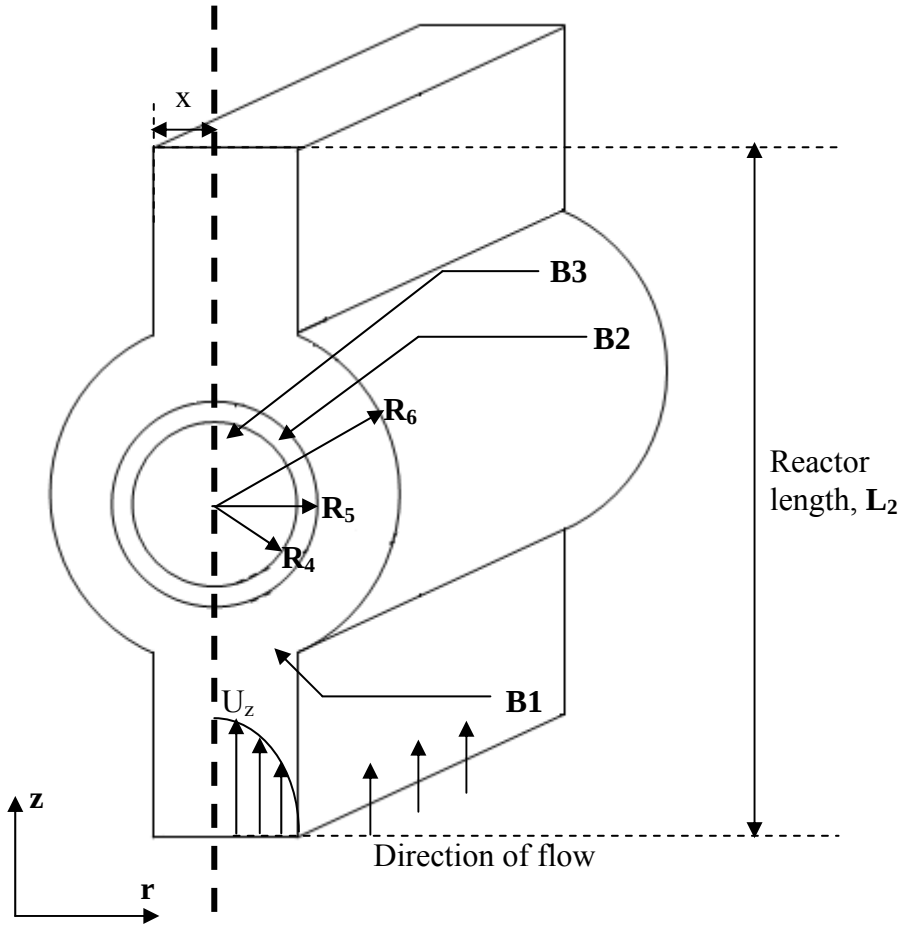

Figure 2- Schematic diagram of the confined perfused bioreactor (CPB) is on the left. On the right are domains defined for nutrient transport modelling in the confined perfused bioreactor. The defined domains are B1-lumen, B2-membrane wall and B3-scaffold construct (with bone cells) respectively. Please refer Table 1 for dimensions.

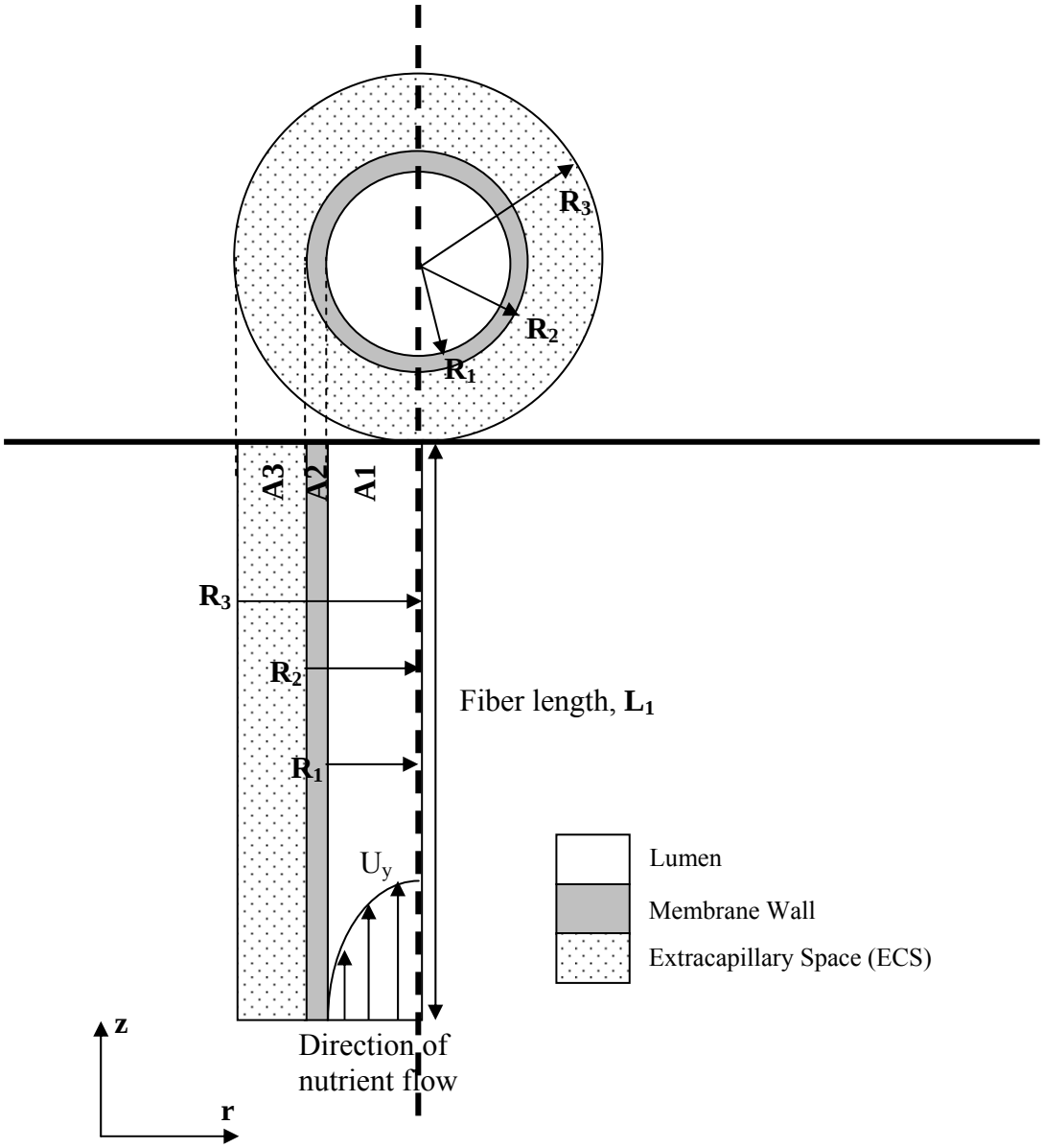

Figure 3- Schematic diagram of a single two dimensional axisymmetrical Krogh cylinder on an is on the top. Below the schematic are domains defined for nutrient transport modelling (via Krogh cylinder approximation) in the hollow fiber membrane bioreactor (HFMB). Three domains are defined, namely A1-fiber lumen, A2-membrane wall and A3-extracapillary space (ECS). Please refer Table 1 for dimensions.

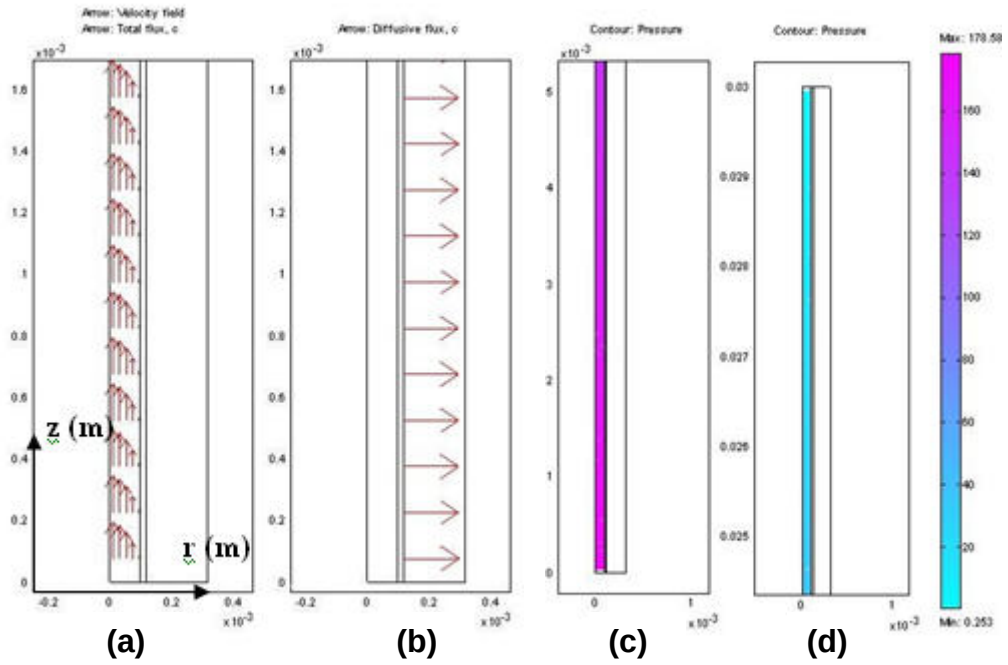

Figure 4- Fluid flow and mass transfer characteristics for hollow fiber membrane bioreactor (HFMB).
(a) Profile of velocity field and concentration flux in the lumen region.
(b) Diffusive flux through the membrane and extracapillary space (ECS) region.
(c) Pressure distribution near the inlet of the lumen (Pa).
(d) Pressure distribution near the outlet of lumen region (Pa).
Characteristics are based on a simulation run for glucose.

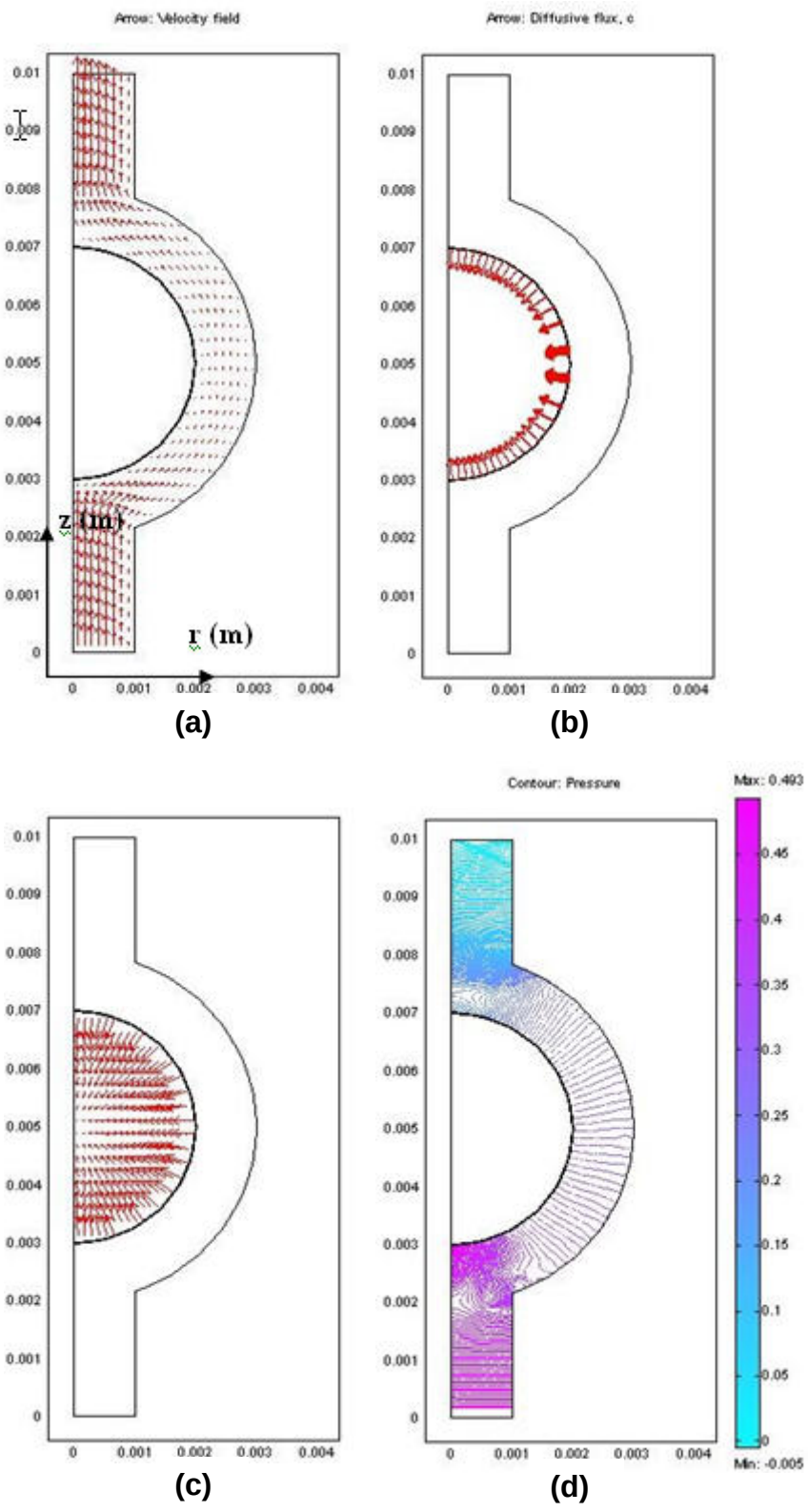

Figure 5- Fluid flow and mass transfer characteristics for confined perfused bioreactor (CPB).
(a) Profile of velocity field and concentration flux in the lumen.
(b) Diffusive flux through the membrane region.
(c) Diffusive flux through the scaffold region.
(d) Pressure distribution in the lumen (Pa).
Characteristics are based on a simulation run for glucose.

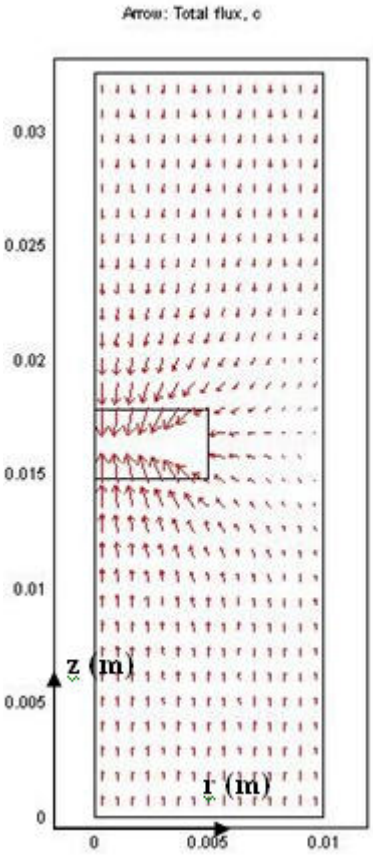

Figure 6- Mass transfer characteristics for suspended tube bioreactor (STB). Arrows in this figure represents flux through the bioreactor.
Characteristics are based on a simulation run for glucose.

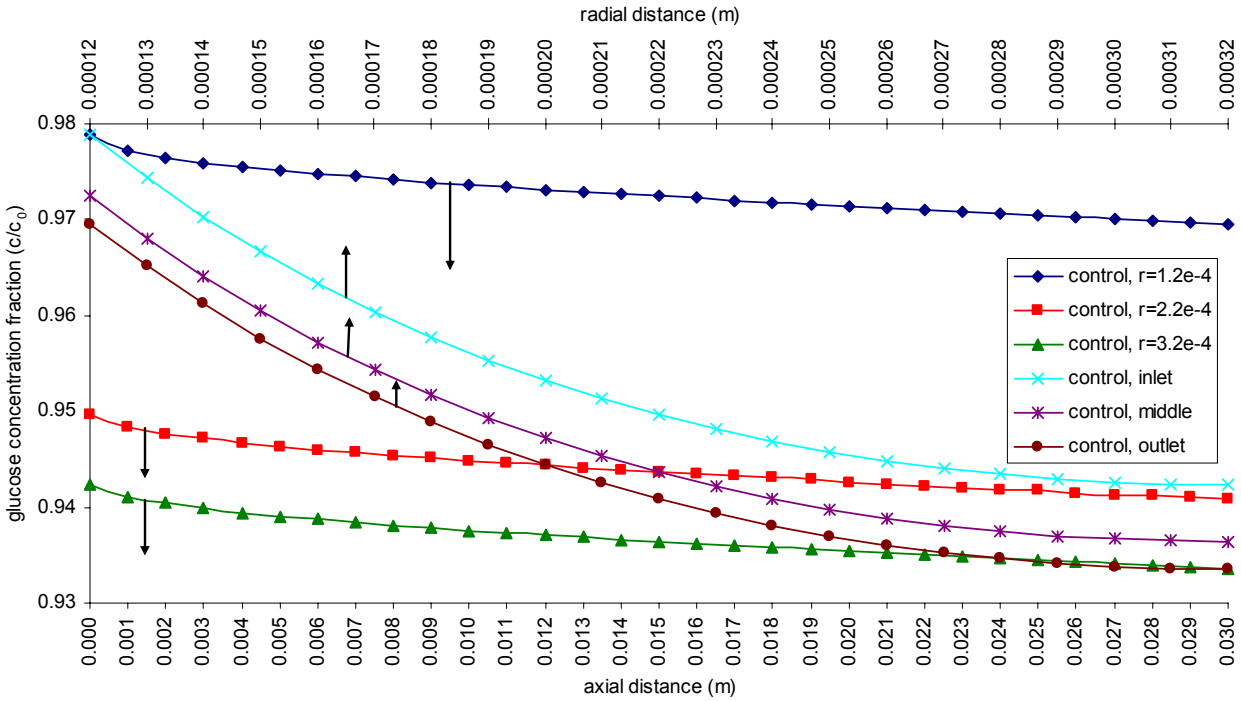

Figure 7- Profiles of axial and radial glucose concentration (mol m^{-3}) in the extracapillary space (ECS) of the hollow fiber membrane bioreactor (HFMB) under control parameters (Refer to Table 1). Axial profiles are displayed at r = 1.2×10^{-4}m (membrane boundary), r = 2.2×10^{-4}m (centre line of extracapillary space) and r = 3.2×10^{-4}m (Krogh cylinder radius). Radial profiles are displayed at z/l = 0 (Extracapillary space boundary adjacent to the bioreactor inlet), z/l = 0.5 (middle of extracapillary space), z/l = 1 (Extracapillary space boundary at outlet of the bioreactor).

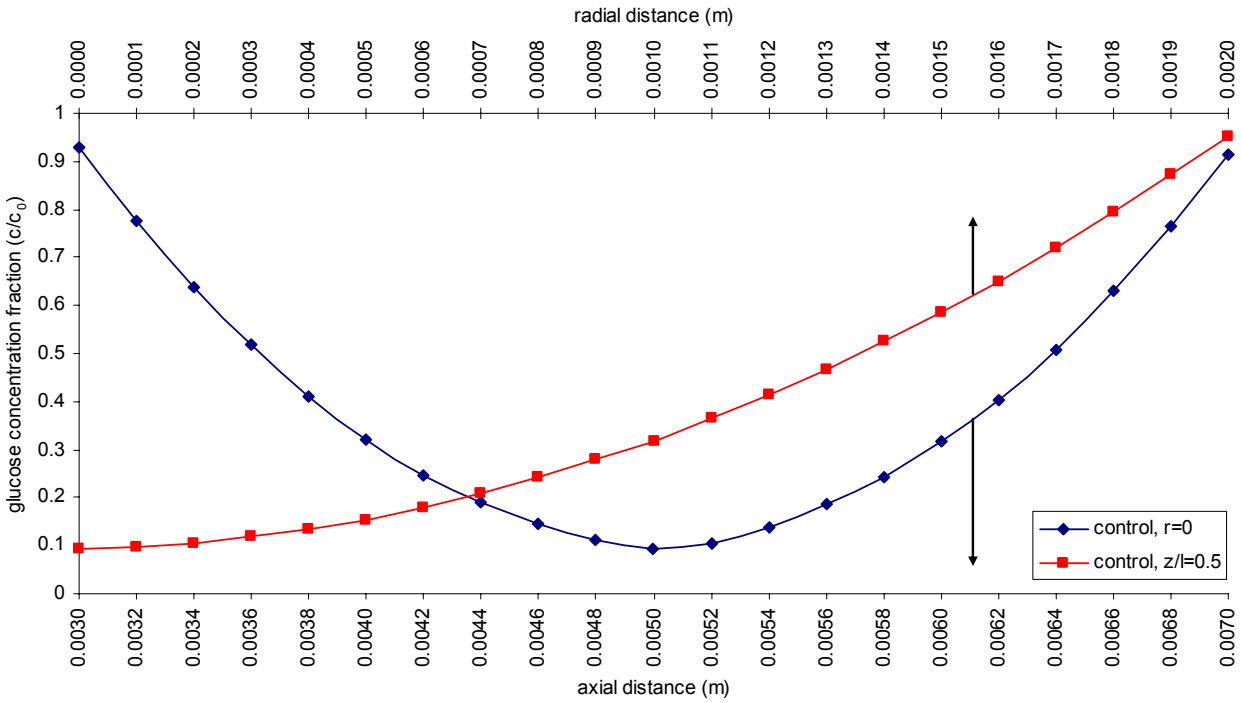

Figure 8- Profiles of axial and radial glucose concentration (mol m^{-3}) in the scaffold construct of the confined perfused bioreactor (CPB) under control parameters (Refer to Table 1). The axial profile is displayed at r = 0 m (central axis of the bioreactor). The radial profile is displayed at z = 0.005m (centre of the bioreactor, z/l = 0.5).

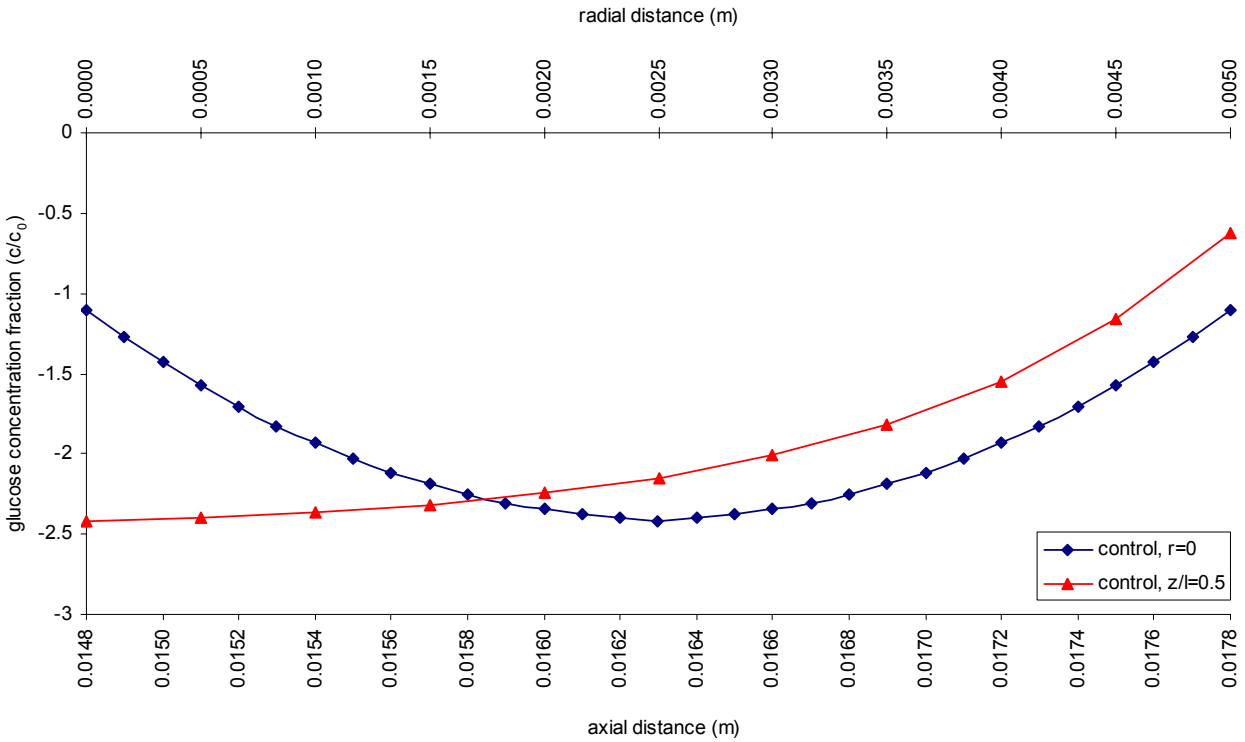

Figure 9- Profiles of axial and radial glucose concentration (mol m^{-3}) in the scaffold of the suspended tube bioreactor (STB) under control parameters (Refer to Table 1). The axial profiles is displayed at r = 0 m (central axis of the bioreactor). The radial profile is displayed at z = 0.0163m (centre of the bioreactor, z/l = 0.5). ('-ve' concentration values imply the amount of glucose deprived from the cells in the scaffold domain).

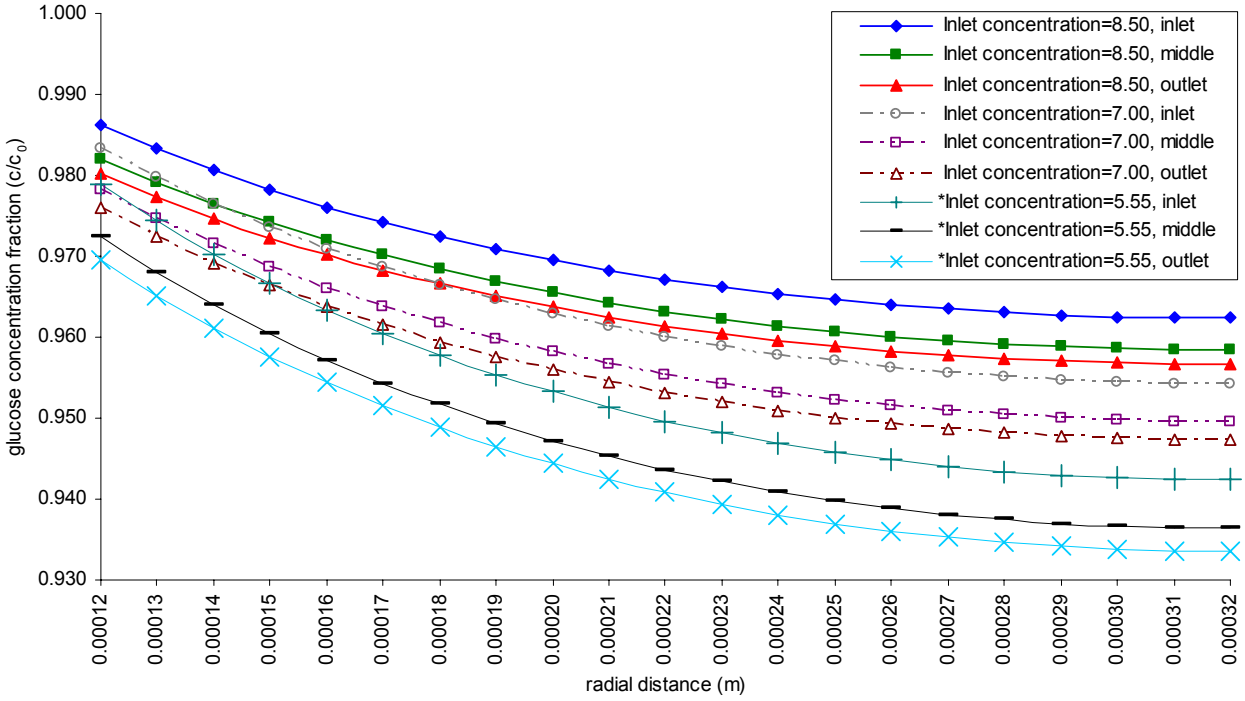

Figure 10- Radial glucose concentration profiles (mol m^{-3}) in the extracapillary space (ECS) of the hollow fiber membrane bioreactor (HFMB) for various inlet glucose concentrations (c_0). Symbol '*' denotes control value of inlet glucose concentration.

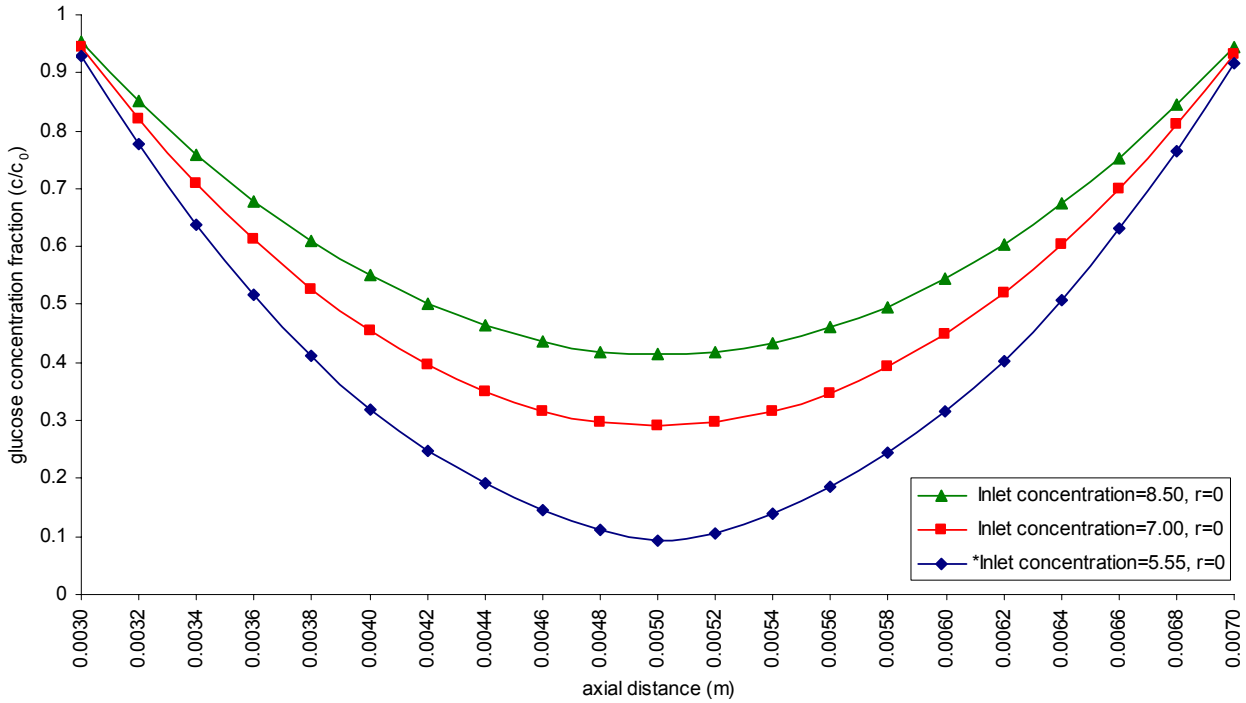

Figure 11- Axial glucose concentration profiles (mol m^{-3}) in the scaffold construct of the confined perfused bioreactor (CPB) for various inlet glucose concentrations (c_0). Symbol '*' denotes control value of inlet glucose concentration.

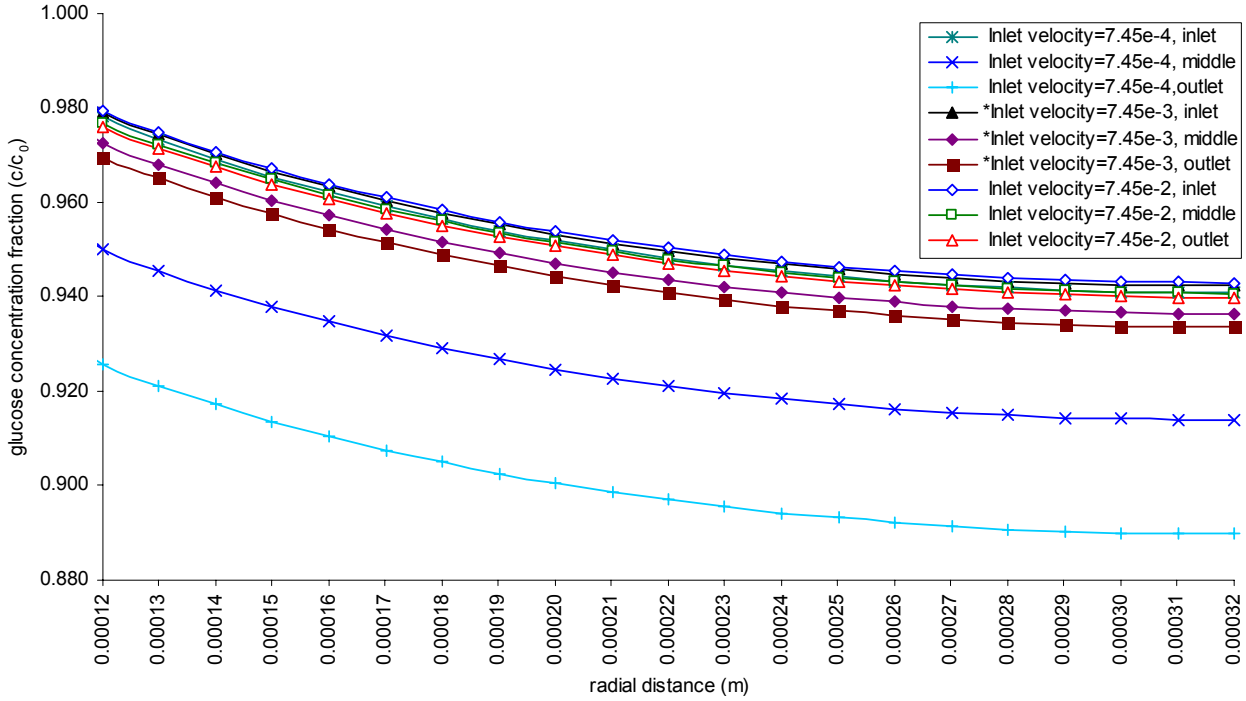

Figure 12- Radial glucose concentration profiles (mol m^{-3}) in the extracapillary space (ECS) of the hollow fiber membrane bioreactor (HFMB) for various inlet velocities (ms^{-1}). Symbol '*' denotes control value of inlet velocity.

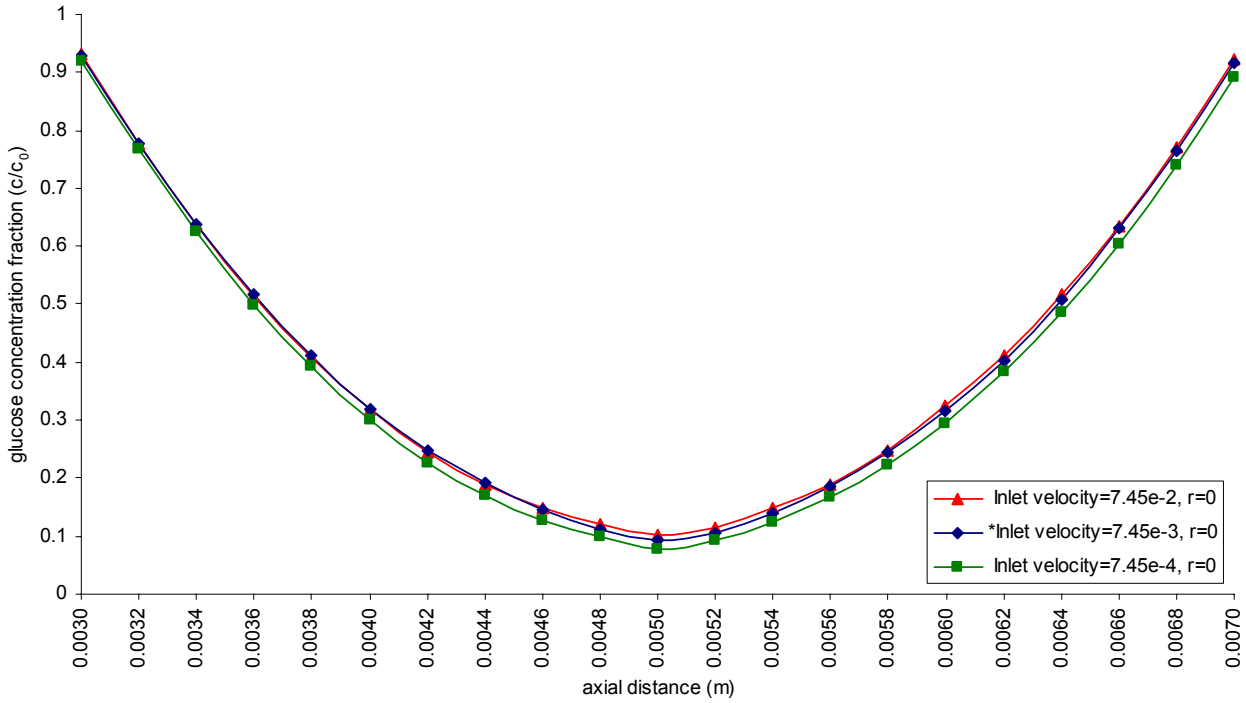

Figure 13- Axial glucose concentration profiles (mol m^{-3}) in the scaffold of the confined perfused bioreactor (CPB) for various inlet velocities (ms^{-1}). Symbol '*' denotes control value of inlet velocity.

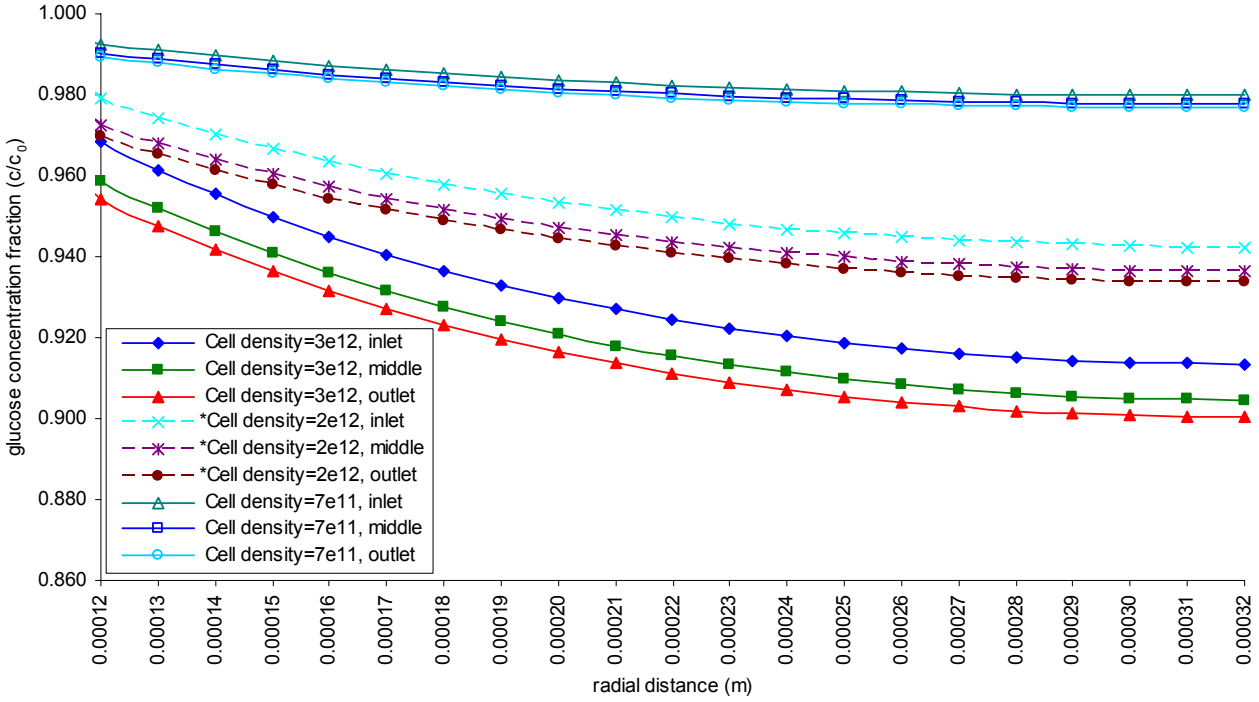

Figure 14- Radial glucose concentration profiles (mol m^{-3}) in the extracapillary space (ECS) of the hollow fiber membrane bioreactor (HFMB) for various cell densities (cells m^{-3}). Symbol '*' denotes control value of cell density.

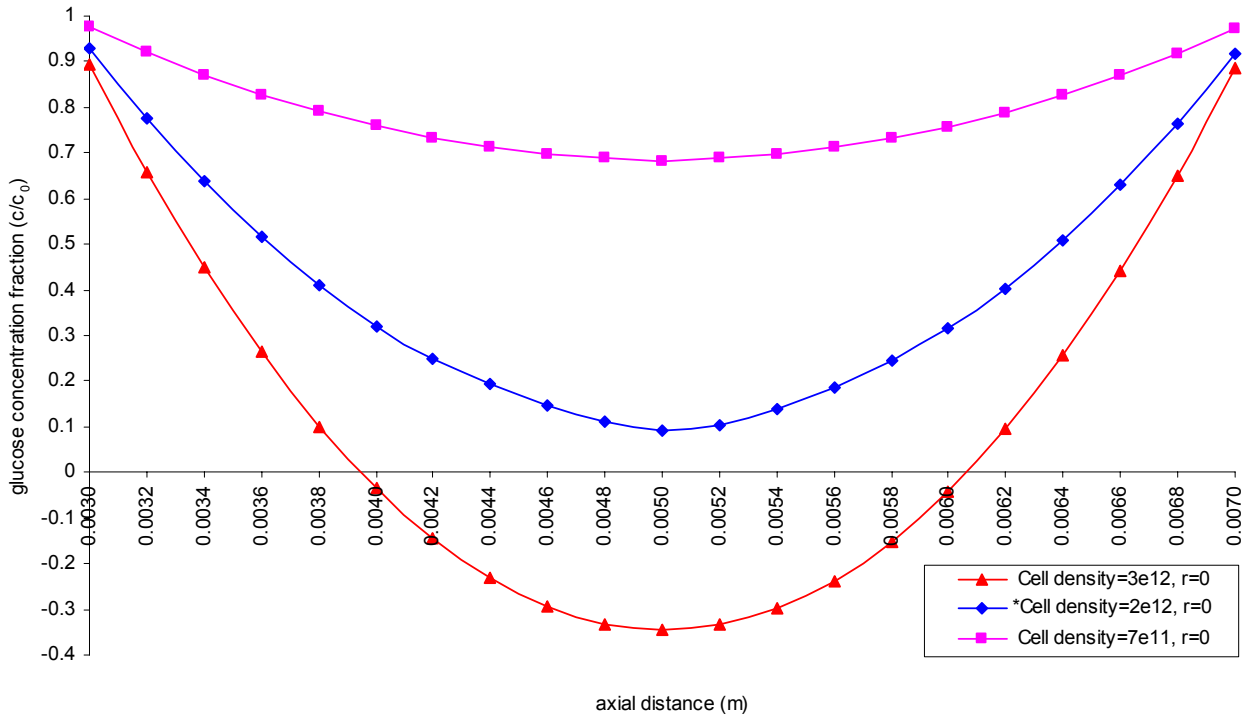

Figure 15- Axial glucose concentration profiles (mol m^{-3}) in the scaffold of the confined perfused bioreactor (CPB) for various cell densities (cells m^{-3}). Symbol '*' denotes control value of cell density. ('-ve' concentration values imply the amount of glucose deprived from the cells in the scaffold domain).

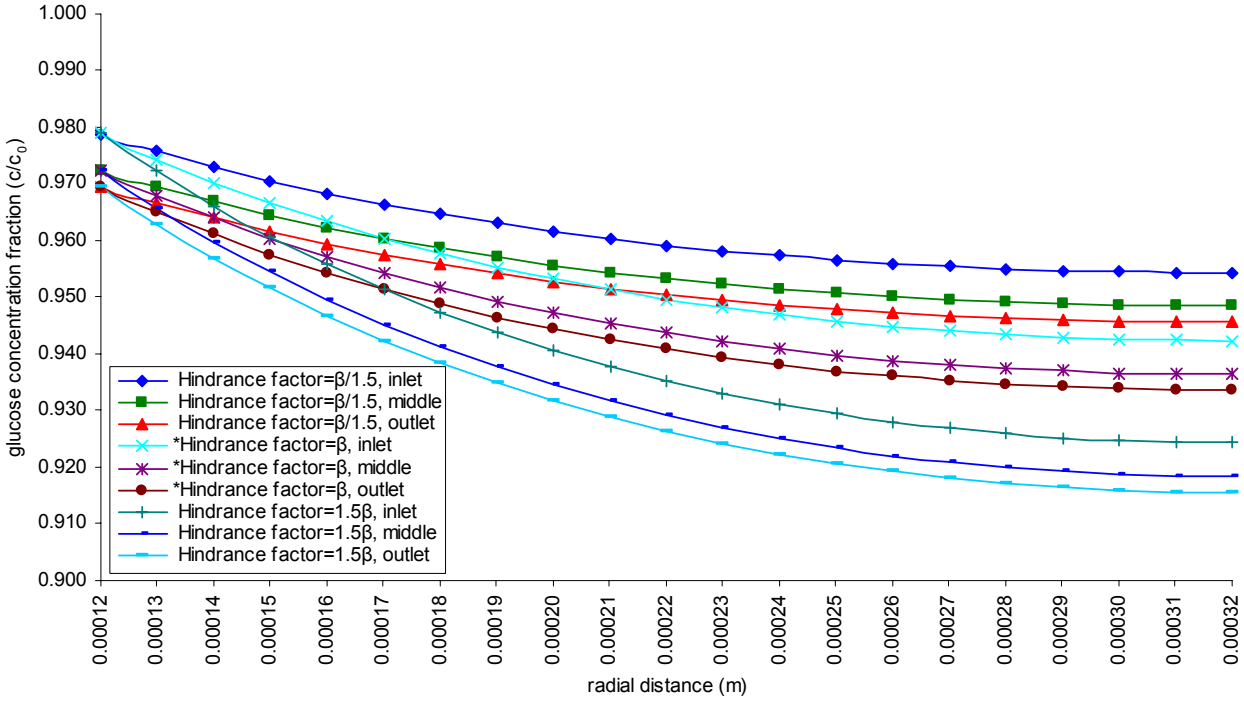

Figure 16- Radial glucose concentration profiles (mol m^{-3}) in the extracapillary space (ECS) of the hollow fiber membrane bioreactor (HFMB) for various scaffold hindering factors (β). Symbol '*' denotes control value of hindering factor (β=5).

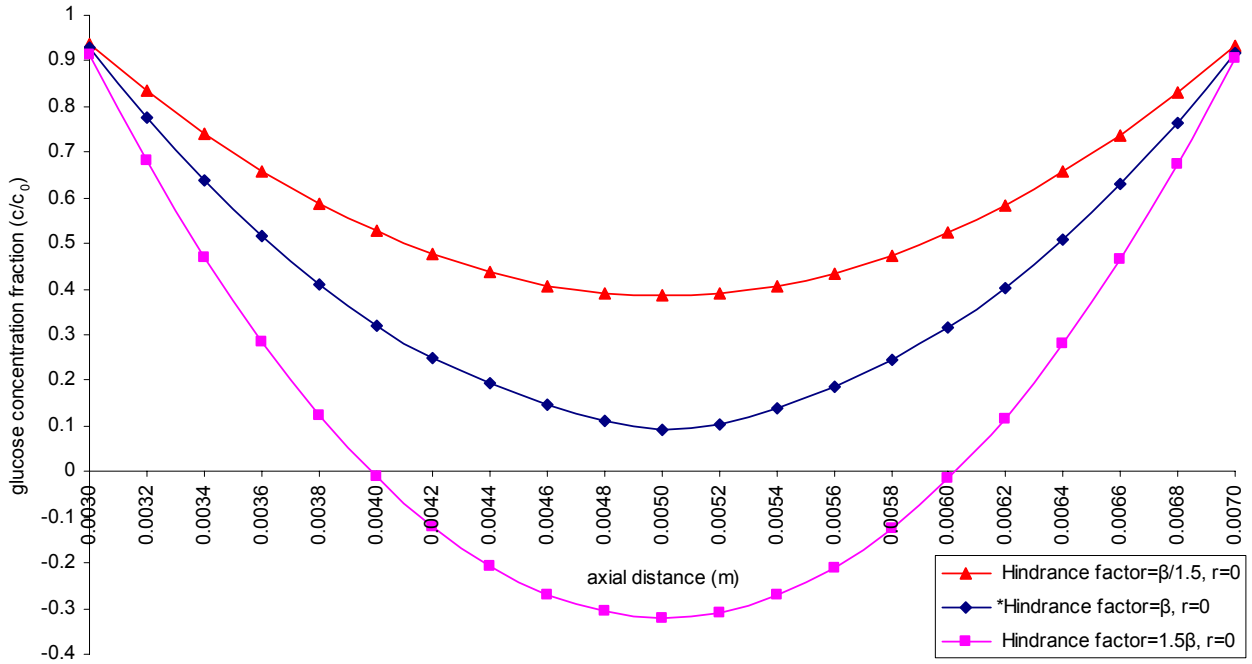

Figure 17- Axial glucose concentration profiles (mol m^{-3}) in the scaffold construct of the confined perfused bioreactor (CPB) for various scaffold hindering factors (β). Symbol '*' denotes control value of hindering factor (β=5). ('-ve' concentration values imply the amount of glucose deprived from the cells in the scaffold domain).